Meteorol. Atmos. Phys. 64, 123–150 (1997)

Meteorology and Atmospheric Physics

[1] Department of Meteorology, Florida State University Tallahassee, Florida, U.S.A.
[2] National Center for Atmospheric Research, Boulder, Colorado, U.S.A.
[3] University of California at San Diego, California, U.S.A.

A High Resolution Global Reanalysis Highlighting the Winter Monsoon. Part I, Reanalysis Fields

T. N. Krishnamurti[1], **B. Jha**[1], **P. J. Rasch**[2], and **V. Ramanathan**[3]

With 25 Figures

Received June 23, 1997
Revised August 6, 1997

Summary

This study entails a reanalysis of the TOGA-COARE, CEPEX period covering the months December 1992 through March 1993. Four times daily data sets were reanalyzed for the period. The unique aspect of this reanalysis is that (i) it incorporates physical initialization i.e. assimilation of rainfall from raingauge and satellite (OLR and microwave radiometric data), (ii) this reanalysis is carried out at a very high resolution, T170, global spectral model (space resolution of roughly 70 km at equator) and (iii) ECMWF reanalysis is used as a first guess field for this study.

This analysis is global and is carried out at 15 vertical levels using the FSU global spectral model. In this study we have analyzed a large number of meterological variables such as wind, temperature, humidity, surface pressure, vertical velocity, cloud, rainfall, surface fluxes and diabatic heating. In this part of the paper we present the monthly mean and samples of daily fields of the reanalysis. Some of the major results of the reanalysis include the relationships among the flow fields and the ITCZ convection; the shallow northeast monsoon current and its rapid turning towards westerlies with height; an overabundance of middle clouds over the region of the ITCZ; and the distribution of heat sources and sinks. A motivation for this reanalysis is the forthcoming Indian Ocean Experiment (INDOEX), which is an international field experiment to be conducted during the winter monsoon time frame in 1999.

1. Introduction

This paper provides the meterological background for a forthcoming field experiment called INDOEX (Indian Ocean Experiment). A list of acronyms appear in Table 1. INDOEX is a joint experiment proposed by a number of countries (USA, Germany, France, India and some others), INDOEX document (Ramanathan et al., 1995, and 1996). The primary objectives of this experiment (INDOEX) are to:

- Assess the significance of sulfates and other continental aerosols for global radiative forcing including the ITCZ cloud system.
- Assess the magnitude of the solar absorption at the surface and in the troposphere including the ITCZ cloud system.
- Assess the role of the ITCZ in the transport of trace species and pollutants and their resultant radiative forcing.

This paper describes the products of a meteorological reanalysis over the globe at very high resolution for a four month period at 6 hourly intervals. These data sets provide a unique

Table 1. *Acronyms*

UTC	Universal Time Coordinated
ECMWF	European Center for Medium Range Weather Forecasts
TOGA-COARE	Tropical Ocean Atmosphere-Coupled Atmospheric Response Experiment
CEPEX	Central Equatorial Pacific Experiment
ITCZ	Inter Tropical Convergence Zone
OLR	Outgoing Longwave Radiation
T170	Triangular truncation T170 wave
FSU	Florida State University
SSM/I	Special Sensor Microwave Images
SST	Sea Surface Temperature
INDOEX	Indian Ocean Experiment
IFA	Intensive Flux Array
SO_2	Sulpher Dioxid
Km	Kilometer
FGGE	First GARP Global Experiment
GARP	Global Atmospheric Research Programme
C^4	Center for Clouds, Chemistry and Climate
COADS	Comprehensive Ocean Atmospheric Data Sets

opportunity for those who wish to examine atmospheric features of this period in more detail than is possible from standard lower resolution reanalysis. Here we present a quick look at the INDOEX meterology from this data set.

The monsoon region, bordered to the south by the vast Indian Ocean and to the north by the densely populated and rapidly developing Indian sub-continent, is a unique laboratory to study the large-scale impact of pollutants on marine tropospheric chemistry and cloud properties. The large scale atmospheric circulation in this region is dominated by a complete annual reversal in the low level winds called the monsoon. This local manifestation of the winter monsoon is fundamentally driven by the differential heating between the Indian sub-continent and the ocean. In the winter months, the atmosphere over the continental areas in the north cools relative to the ocean, forming a region of general subsidence. A high pressure system which forms over central India gives rise to the Indian dry season and generates a persistent northeasterly offshore flow. During these northern winter months (December–March), the cross equatorial monsoonal flow may provide a mechanism by which the northern hemisphere air, laden with continental aerosols, anthropogenic sulfates and reactive gases, is coupled to the relatively pristine air of the southern hemisphere at the conflux of the two air masses into the ITCZ.

2. The Analysis Procedure – Physical Initialization

The reanalysis of the data in this study is based on physical analysis procedures developed at

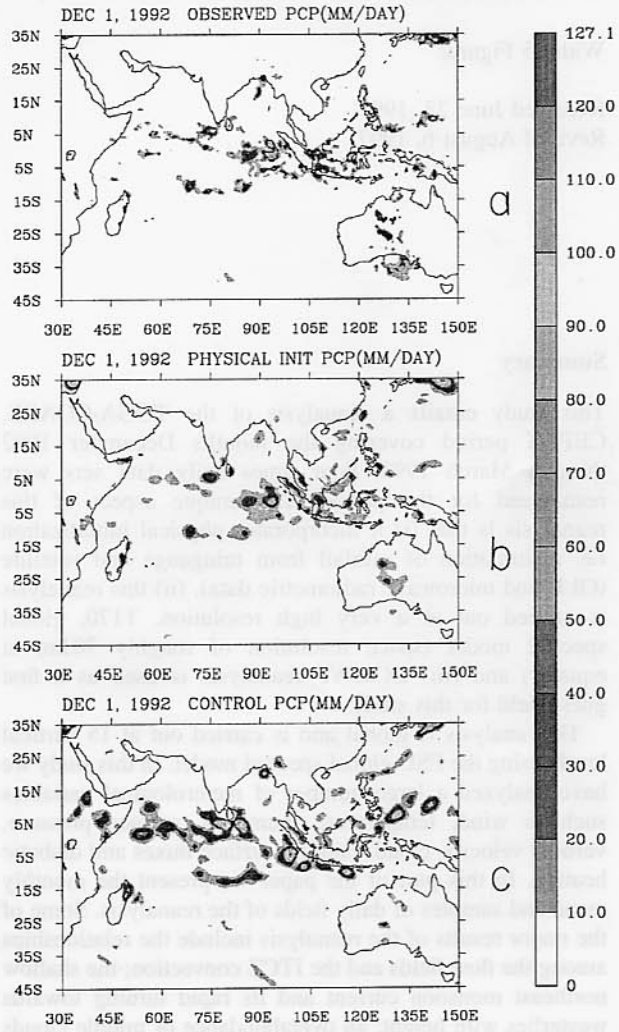

Fig. 1. 24 hours rainfall ending on December 1, 1992 at 12 UTC (a) based on satellite plus raingauge observation (b) based on physical initialization (c) based on control experiment. Units: mm/day; The rainfall amounts over shaded areas are according to the scale shown at the right

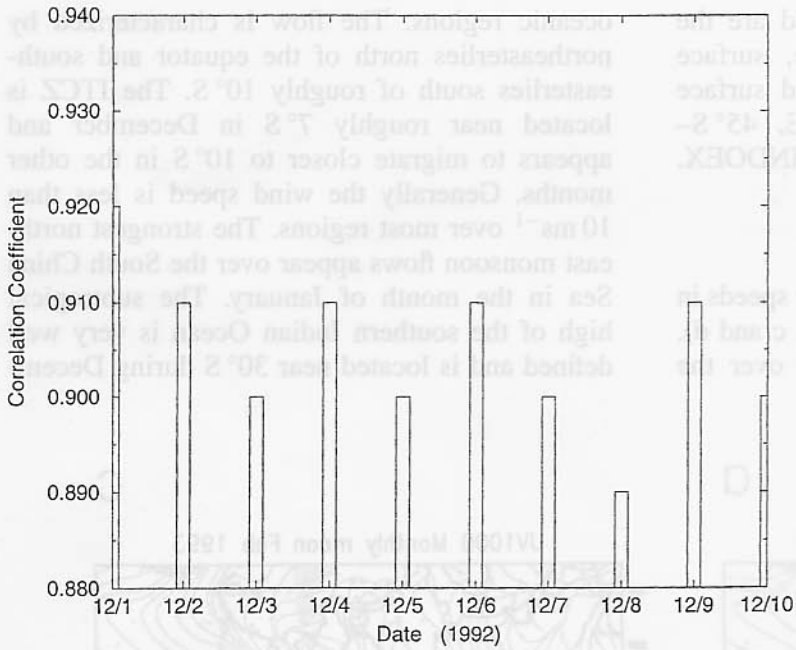

Fig. 2. Global tropical rainfall correlation between physical initialization and observation for the period 1 December 1992 to 10 December 1992

FSU (Krishnamurti et al., 1991). In this study we present the reanalyzed products for the four months December 1992 through March 1993. Physical initialization was performed using a very high resolution (T170) global model; see Appendix 1 of Part 2 (Krishnamurti et al., 1997) for an outline of the model. The observed rainfall used during physical initialization was based on surface and satellite rainfall as described in Gairola and Krishnamurti (1992). The physical initialization involves rainfall and OLR assimilation using several reverse algorithms:

a) a reverse cumulus parameterization
b) a reverse surface similarity, and
c) a matching of the outgoing longwave radiation where the model based values are relaxed towards satellite based values.

The entire process restructures the humidity profiles along the vertical and spins up the convective heating, divergence and the related fields consistent with the observed rain rates.

Figure 1 (a, b, c) illustrates a typical spin-up of the rainfall via physical initialization. Here the top panel illustrates the 24 hour rainfall (between November 30 and December 1 1992, 12 UTC). These values are based on a mix of SSM/I, OLR rainfall and data from the surface raingauge network. The middle panel shows what is recovered by the assimilation invoking physical initialization. The data represented in these two panels (top and middle) have a correlation of around 0.9. That level of correlation has been noted on a daily basis, see Fig. 2. The bottom panel (Fig. 1c) illustrates the 24 hour rainfall total from a control experiment which did not involve any physical initialization. The correlation between this field and the 'observed' rainfall is typically around 0.4. Thus the physical initialization is able to assimilate the observed rainfall very well. The diabatic heating and divergence fields evolve during the physical initialization consistent with the improved rain rates. The surface fluxes also become well defined with robust air-sea coupling. This reanalysis, therefore, we feel is dynamically and thermodynamically much more consistent than the original ECMWF analysis.

3. Winter Monsoon Climatology

Under this section we shall present mean monthly fields of selected variables which are representative of the climatology of the winter

monsoon domain. The fields presented are the wind, rainfall, SST, air temperature, surface humidity, clouds, diabatic heating and surface fluxes over the region 30° E–150° E, 45° S–35° N, which is an area of interest for INDOEX.

3.1 1000 mb flow Field

Here the streamline field is shown (with speeds in excess of 10 ms^{-1} shaded), Fig. 3 (a, b, c and d). The essential features of interest are over the oceanic regions. The flow is characterized by northeasterlies north of the equator and southeasterlies south of roughly 10° S. The ITCZ is located near roughly 7° S in December and appears to migrate closer to 10° S in the other months. Generally the wind speed is less than 10 ms^{-1} over most regions. The strongest northeast monsoon flows appear over the South China Sea in the month of January. The subtropical high of the southern Indian Ocean is very well defined and is located near 30° S during Decem-

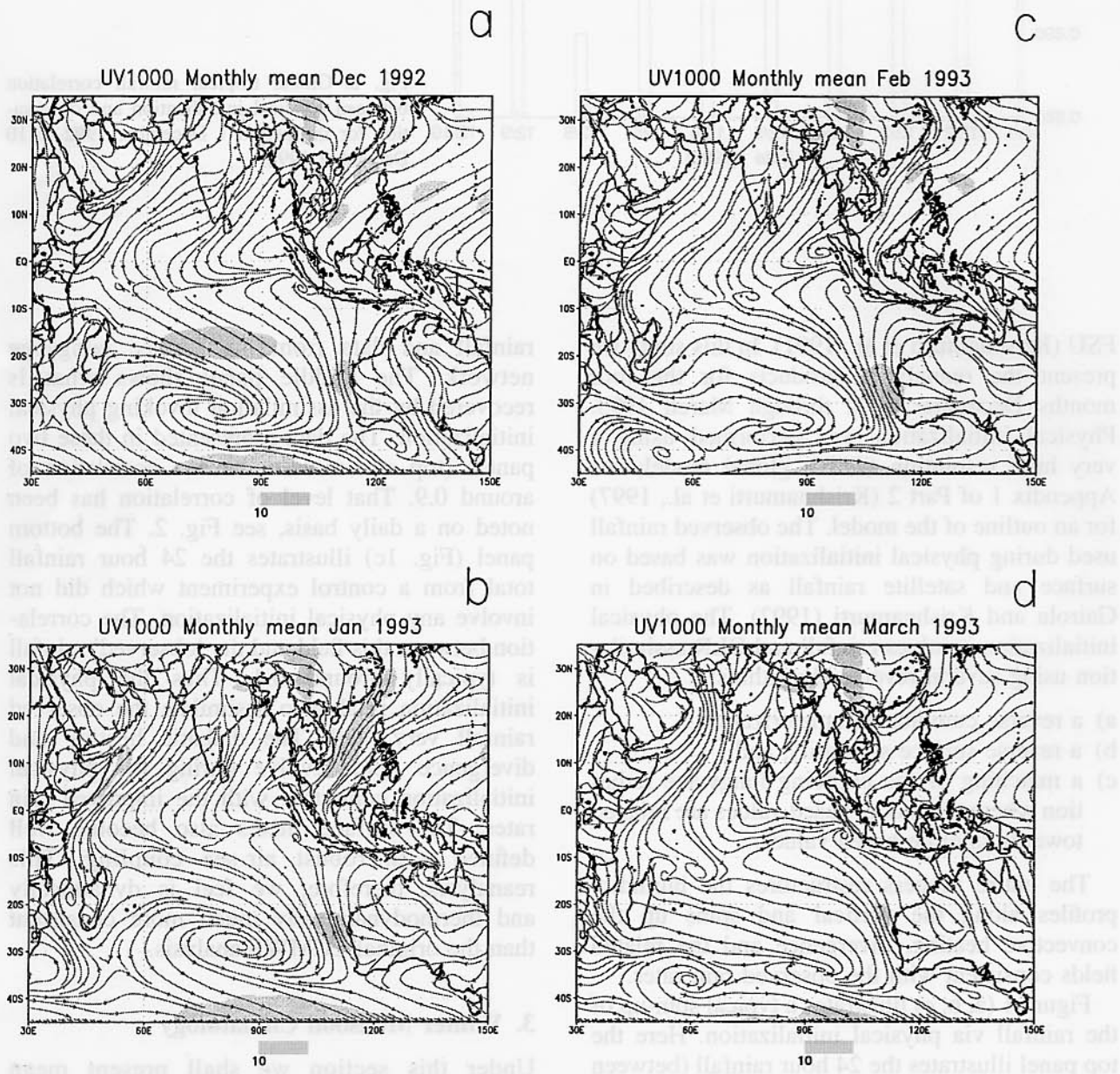

Fig. 3. Monthly mean streamline and isotachs at 1000 mb for (a) December 1992, 12 UTC (b) January 1993, 12 UTC (c) February 1993, 12 UTC, (d) March 1993, 12 UTC. Units: ms^{-1}; shaded area indicates wind speed $\geq 10\,ms^{-1}$

ber and January but appears to migrate southward during February and March close to 35° S, is much narrower in the meridional direction, and is imbedded in a strong shear zone.

3.2 850 mb flow Field

The salient difference between the 1000 mb and the 850 mb flows (close to 1.5 km above the ocean) Fig. 4 (a, b, c and d) is a rapid turning (veering) of the winds with height. The flows over the Arabian Sea have a much stronger easterly component. Over the northern Bay of Bengal the winds show a strong anticyclonic turn (more northerly over land and an easterly turn over the ocean). The continental pollution (from near 20° N and 90° E) at 850 mb would move towards the east coast of Africa prior to a sharp southward turn towards the oceanic ITCZ. The surface flows, however, have a better chance of conveying the pollutants directly towards the ITCZ over the central Indian Ocean. In general

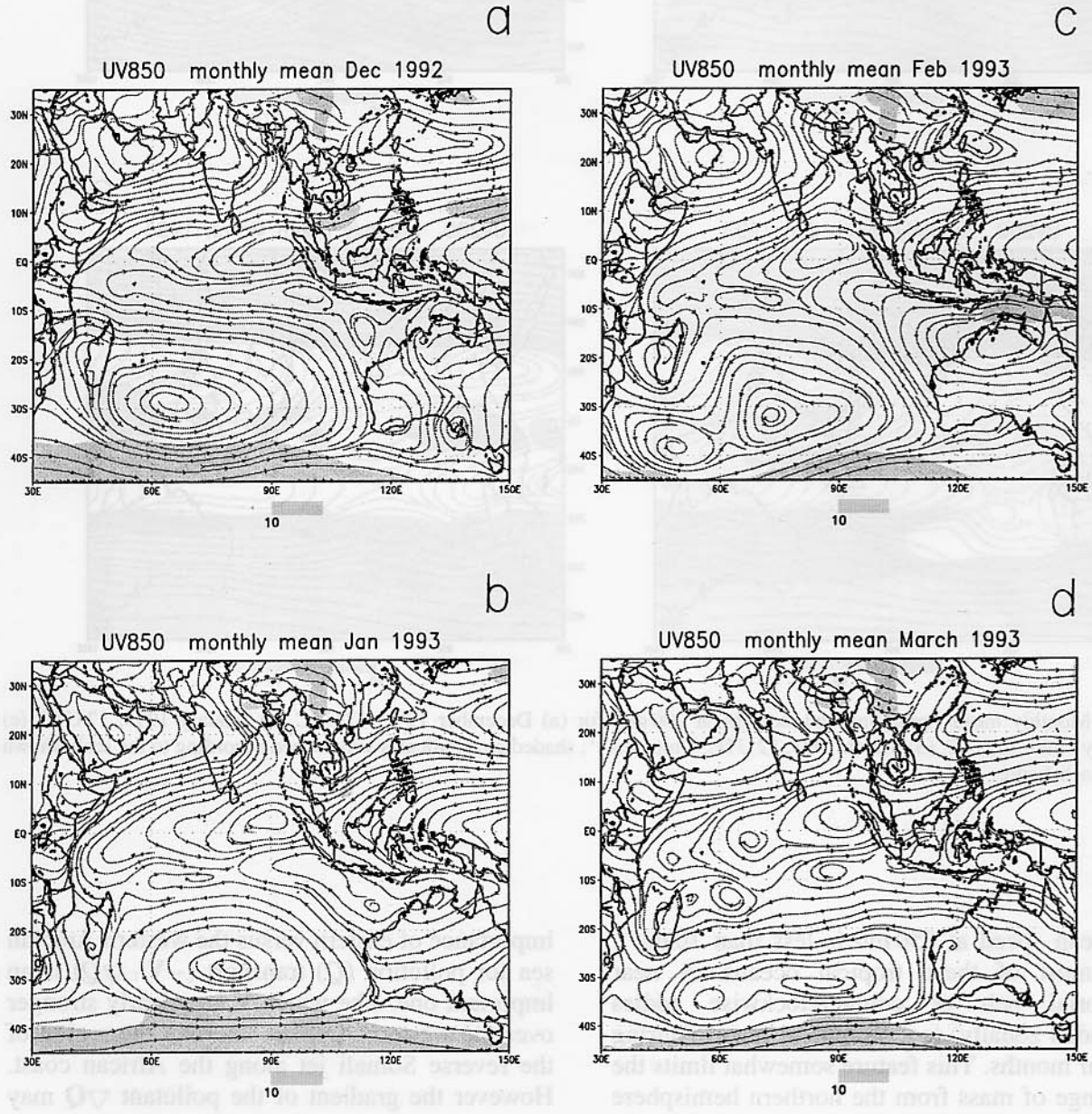

Fig. 4. Monthly mean streamline and isotachs at 850 mb, for (a) December 1992, 12 UTC (b) January 1993, 12 UTC (c) February 1993, 12 UTC, (d) March 1993, 12 UTC. Units: ms^{-1}; shaded area indicates wind speed $\geq 10\,ms^{-1}$

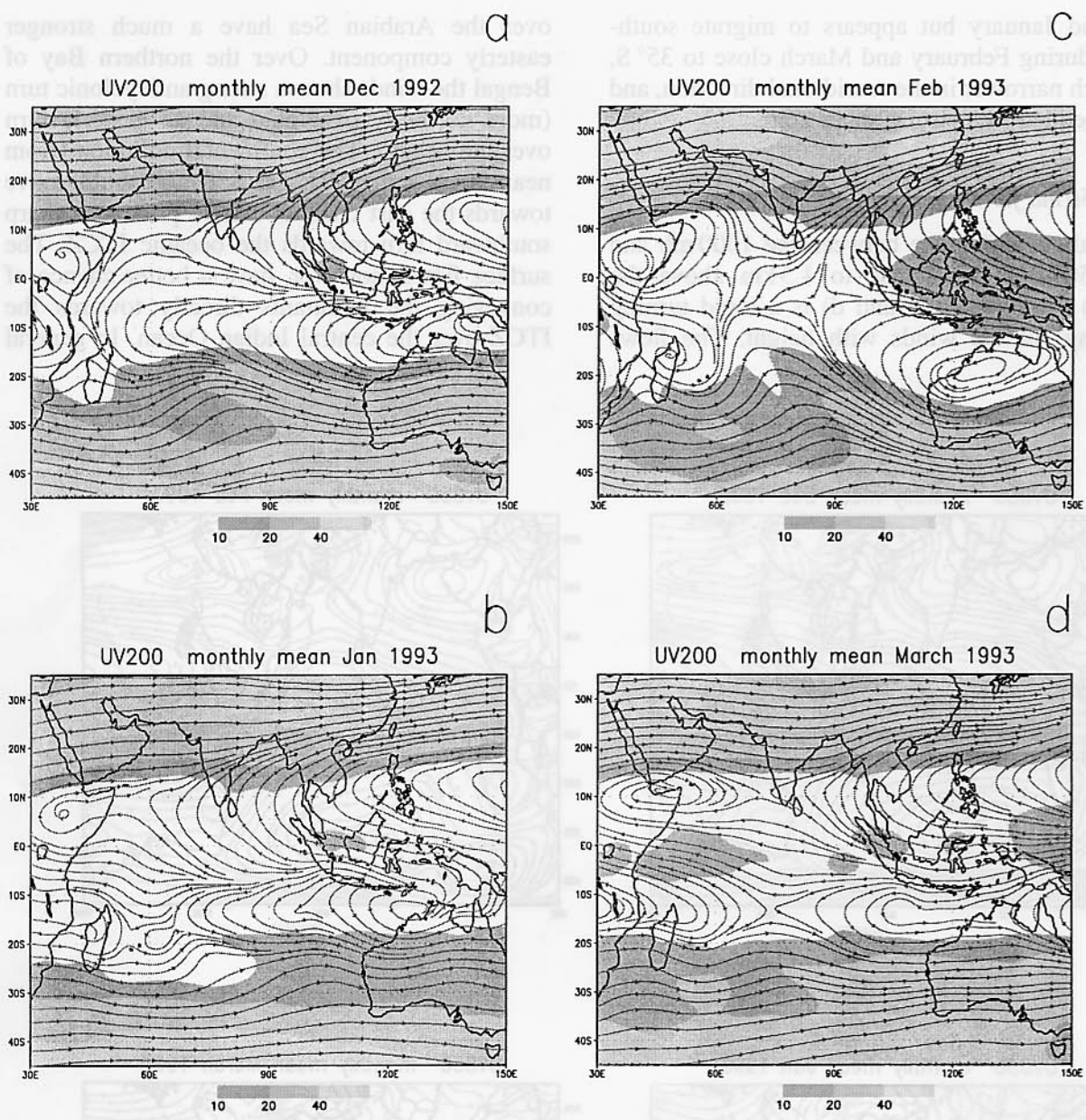

Fig. 5. Monthly mean streamline and isotachs at 200 mb, for (a) December 1992, 12 UTC (b) January 1993, 12 UTC (c) February 1993, 12 UTC, (d) March 1993, 12 UTC. Units: ms^{-1}; shaded area indicates wind speed according to the scale shown below each figure

the mean speed at 850 mb is less than 10 ms^{-1} over most of these tropical oceans. A near equatorial belt of counterclockwise eddies (extended zonally) is a prominent feature during all four months. This feature somewhat limits the exchange of mass from the northern hemisphere to the ITCZ, which is located to the south of this belt of counterclockwise eddies. The issue on the importance of eastern versus the western Arabian sea for pollution (Q) transport ($-\mathbf{V} \cdot \nabla Q$) is an important one. The winds $\mathbf{V}$ are clearly stronger over the western Arabian sea over the region of the reverse Somali jet along the African coast. However the gradient of the pollutant $\nabla \mathbf{Q}$ may be largest near the source region, i.e. near the coast of India, thus one is confronted with the

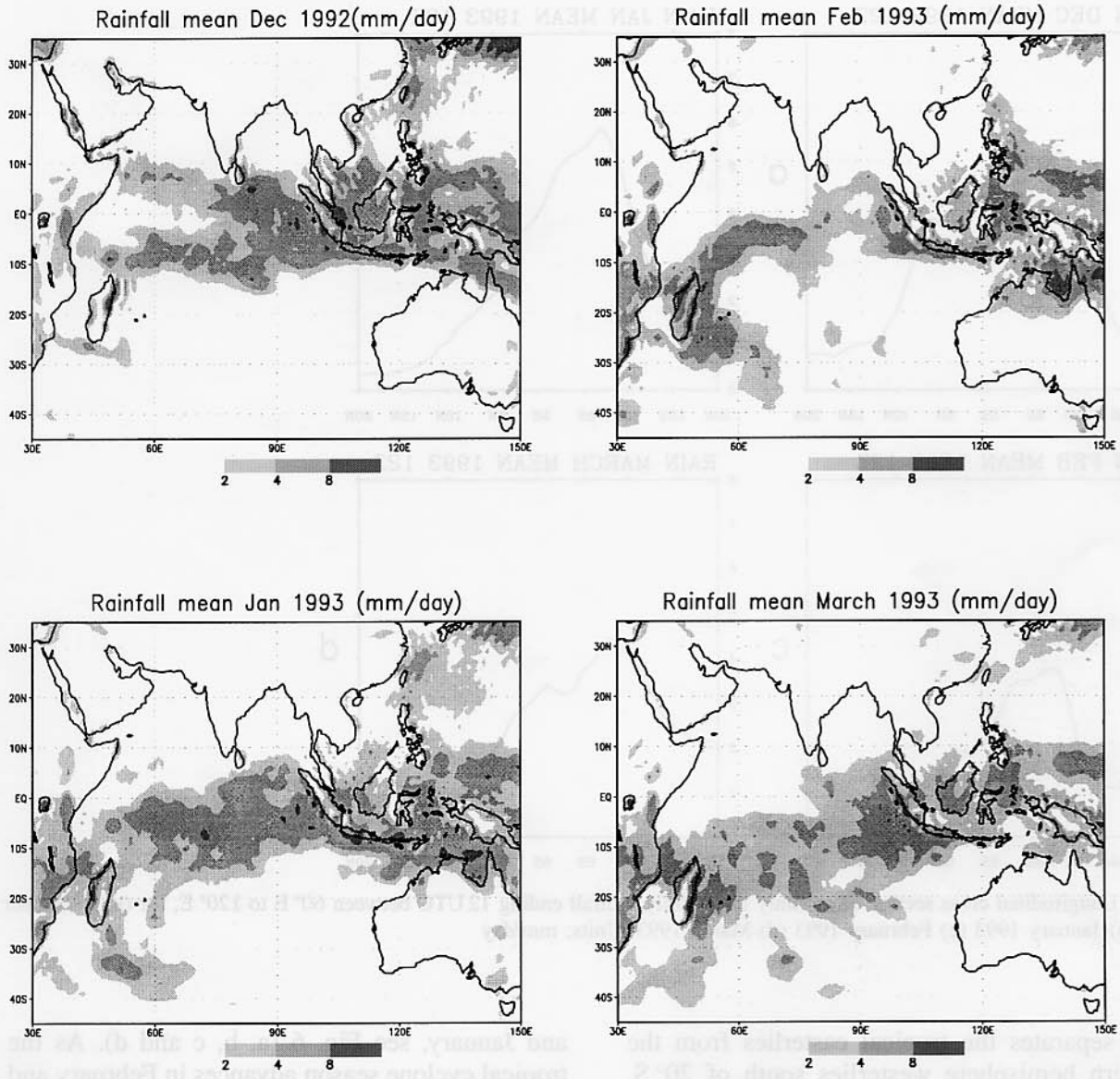

Fig. 6. Monthly mean daily rainfall ending 12 UTC, for (a) December 1992 (b) January 1993 (c) February 1993 (d) March 1993. Units: mm/day; the rainfall amounts over shaded areas are according to the scale shown below each figure

more important issue where in the end the transports are most effective. The Arabian desert aerosols appear to be most effectively transported down the Arabian sea coast of North Africa. The pollution for India, however, is clearly another story. Thus, a careful monitoring of the eastern, western and the central Arabian sea may be necessary during INDOEX. The east African highlands have a strong influence in keeping the reverse Somali jet offshore over the Western Arabian Sea.

3.3 200 mb Flows

An axis of anticyclonic flows Fig. 5 (a, b, c and d) separates the westerlies north of 10° N from the tropical easterlies near the equatorial latitudes. Another belt of anticyclones locates near

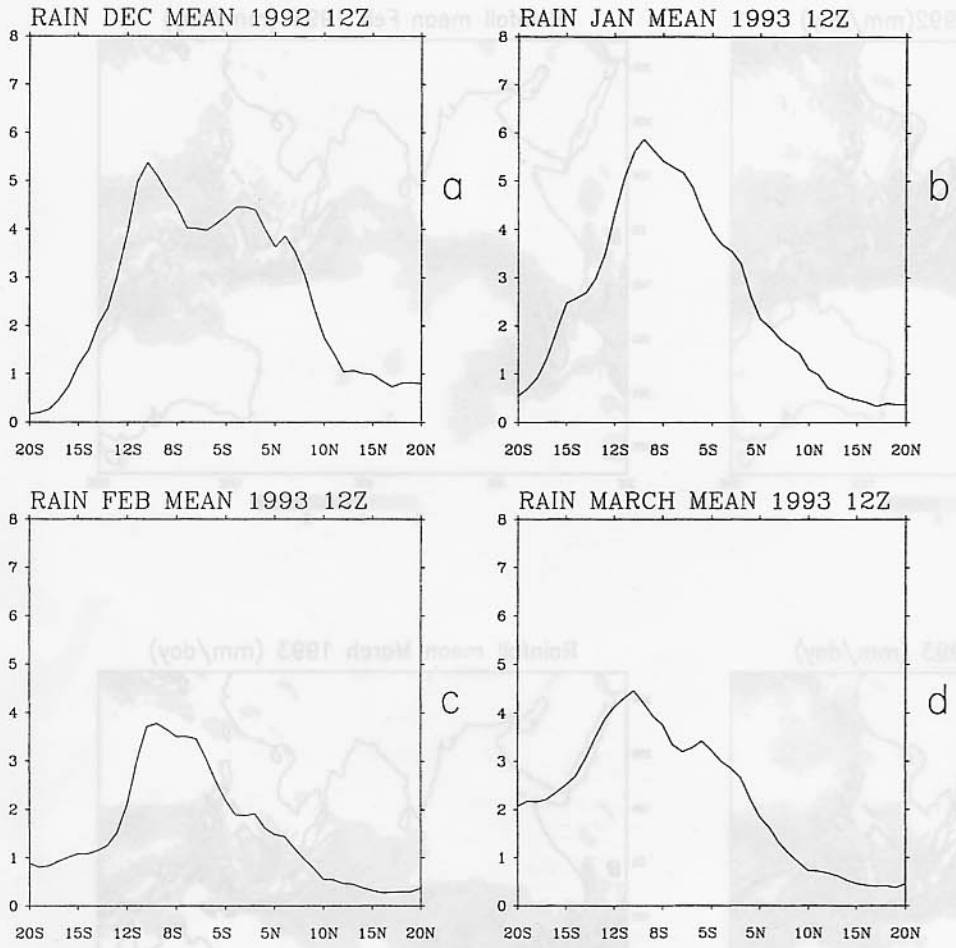

Fig. 7. Longitudinal cross section of monthly mean daily rainfall ending 12 UTC between 60° E to 120° E, for (a) December 1992 (b) January 1993 (c) February 1993 (d) March 1993. Units: mm/day

10° S separates the tropical easterlies from the southern hemisphere westerlies south of 20° S. The region between these two prominent belts of anticyclones is a general region of flow diffluence. Here this diffluence characterizes the outflow region of the ITCZ. Thus any pollutants carried upwards by convection are equally likely to be conveyed to the northern or the southern hemisphere in these outflowing diffluent regions. The outflowing wind speeds over the ITCZ are generally weak and are less than $10\,ms^{-1}$.

3.4 Monthly mean Precipitation

Precipitation is estimated from the microwave-based algorithms of SSM/I over the oceans and raingauge and OLR over land (Gairola and Krishnamurti, 1992). The axis of heavy rainfall extends zonally along 10° S during December and January, see Fig. 6 (a, b, c and d). As the tropical cyclone season advances in February and March, heavy precipitation amounts are noted along the Madagascar coast where the tropical systems exhibit a recurvature. The principal axis of precipitation extends from southwest to northeast across the Indian Ocean. In general, precipitation amounts along the ITCZ (for the monthly mean) are of the order 5 to 10 mm/day. In December, the maximum rainfall east of 80° E extends over a broad belt both north and south of the equator between 10° N and 10° S. With the advance of the winter season this feature north of the equator weakens considerably. A zonal average of the monthly mean rainfall across the Indian ocean between 60° E and 120° E as a function of latitude is presented in Fig. 7 (a, b, c and d). A prominent peak near 10° S denotes the rainfall associated with the ITCZ. This peak also

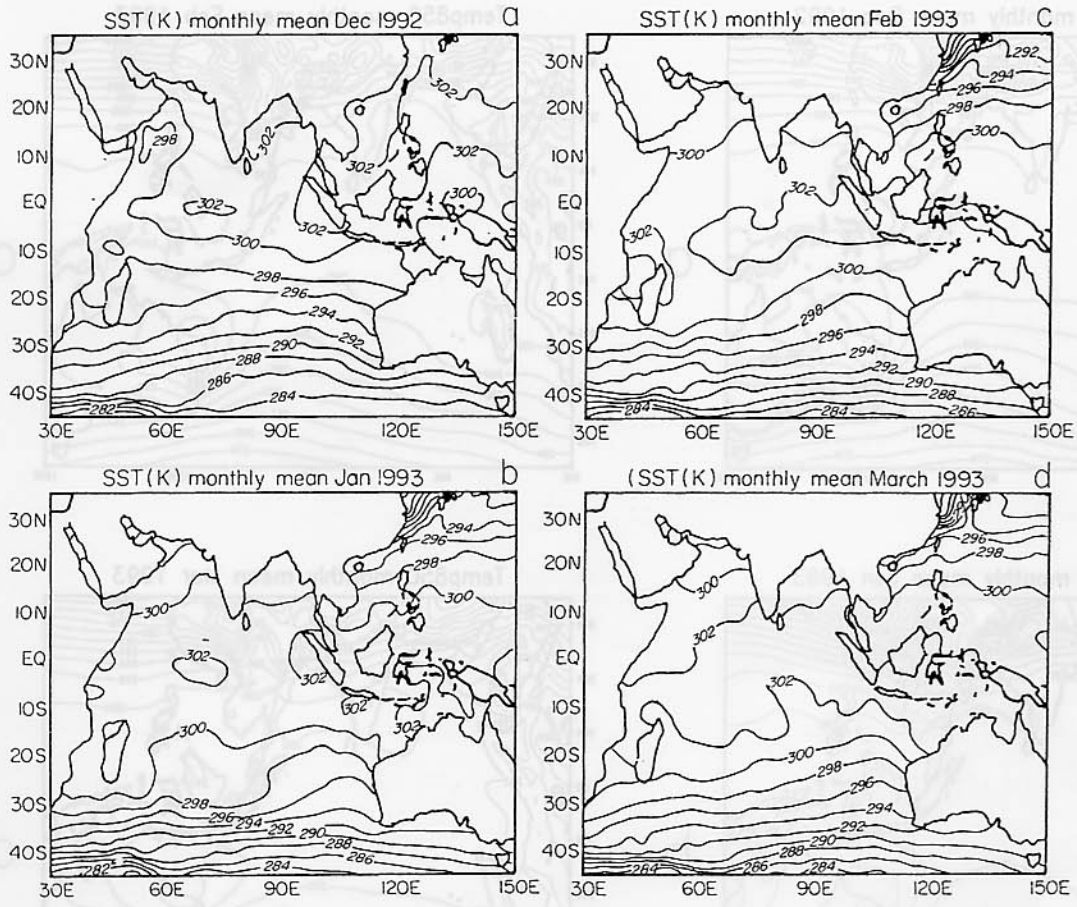

Fig. 8. Monthly mean Sea Surface Temperatures (SST), for (a) December 1992, 12 UTC (b) January 1993, 12 UTC (c) February 1993, 12 UTC, (d) March 1993, 12 UTC. Units: K; contours interval: 2 K

reflects the average of heavy rainfall arising from westward propagating disturbances along the ITCZ. During December a secondary broad maximum extends from 5° S to 5° N which is related to the activity over the Bay of Bengal, South China Sea, Java Sea and the Western Pacific Ocean. This bimodal feature is not evident in the monthly mean fields of zonally averaged rainfall during January and February. A peak near 12° S largely arises from disturbance activity to the south of the ITCZ. During March a bimodality in the Southern hemisphere is related to an ITCZ near 7° S and disturbance activity near 12° S. The zonally averaged maximum rainfall amounts are of the order of 3 to 6 mm/day.

3.5 Sea Surface Temperatures (SSTs)

The Indian Ocean contains a large extent of warm water, with an areal coverage somewhat less than the Western Pacific warm pool. Monthly mean sea surface temperatures (SSTs), Fig. 8 (a, b, c and d), over the equatorial Indian Ocean (5° N to 5° S) are in the range of 301° K to 302° K. Since deep convection is generally triggered over such warm waters, this region also has an important role in the diabatic forcing of the winter monsoon circulation. The cross equatorial low level flow into this region of deep convection is associated with the ITCZ. The deep convection along the ITCZ is manifested by an abundance of cloud cover, Figs. 11–14 which contributes significantly to the vertical exchange of aerosols and trace gases between the surface and upper troposphere including possibly the lower stratosphere. The meridional temperature gradients of SST over the northern Arabian sea and the Bay of Bengal are much weaker than those for the air temperatures shown in Fig. 9 (a, b, c and d). Continental air passing over these

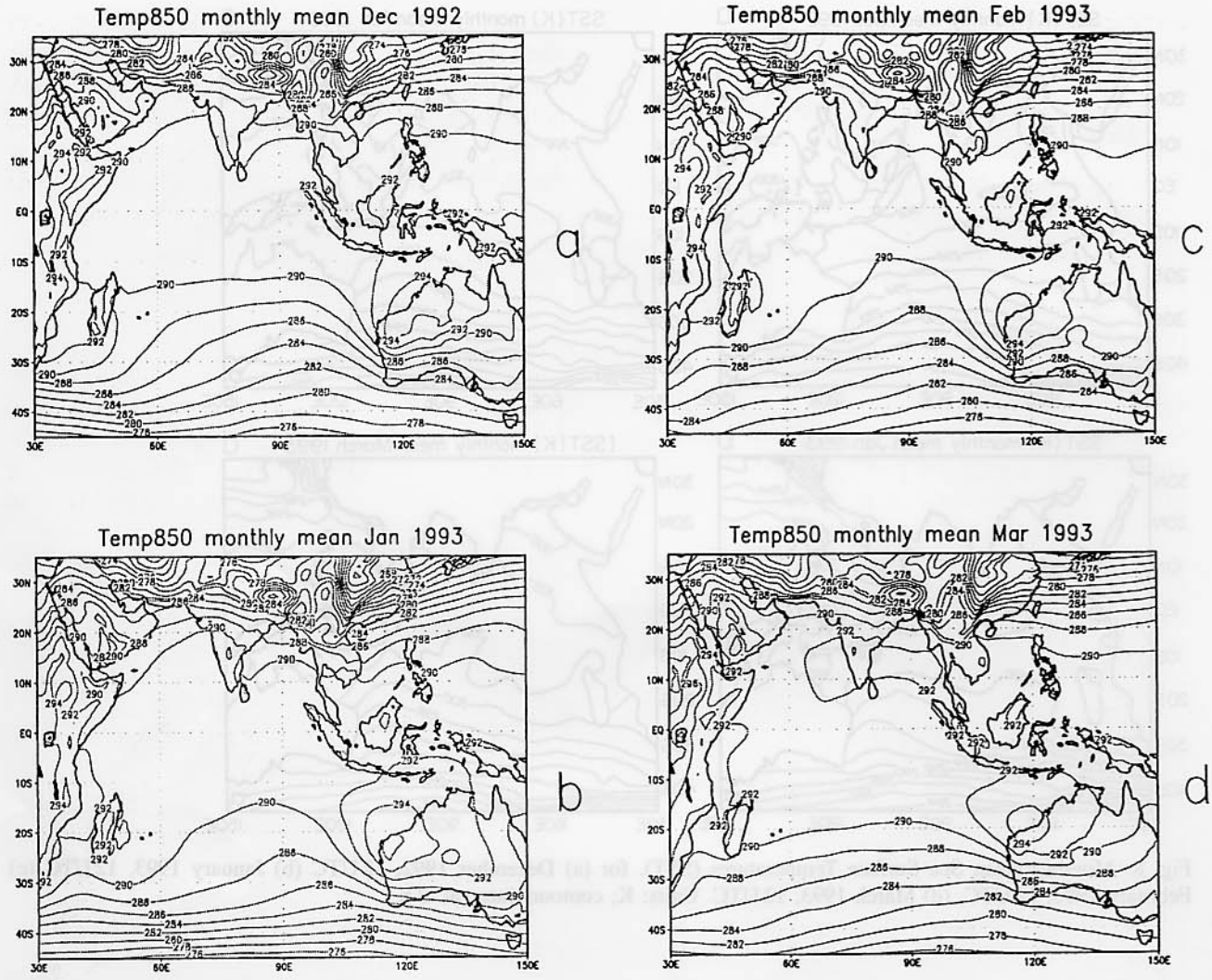

Fig. 9. Monthly mean air temperature at 850 mb, for (a) December 1992, 12 UTC (b) January 1993, 12 UTC (c) February 1993, 12 UTC, (d) March 1993, 12 UTC. Units: K; contours interval: 2 K

oceans is colder than the SST. A rapid air sea exchange of sensible and latent heat is noted as the northerly flow traverses over these regions. Over most of the equatorial belt 10° S to 10° N the SST is only about a degree warmer than the surface air temperature. The largest values of SST over the equatorial belt are of the order 302 K (29 °C).

3.6 Lower Tropospheric Thermal Field

In general the thermal fields over the Indian Ocean are very uniform in these monthly mean representations. Figure 9 (a, b, c, d) illustrates the 850 mb thermal fields during the months December through March. In general the tropical belt between 10° S to 10° N shows a temperature of around 290 K to 291 K at 850 mb. Warmest air resides over north-western Australia. The monthly mean temperature fields over the Indian subcontinent are quite similar at 850 mb during the months December, January and February. During March a warming over Southern India indicates the beginning of the transition towards the spring warming. North of 10° N the thermal wind is consistent with the observed strong

turning of winds from west to east above the 850 mb level.

3.7 Surface Humidity Field

This is an important field in the winter monsoon scenario. Here we see values below 10 g/kg, Fig. 10 (a, b, c and d), near 20° N and as high as 21 g/kg over the general region of the ITCZ. Sharp meridional gradients over land in the northern hemisphere and over the ocean in the southern hemisphere are noted during the entire season. Values of surface specific humidity in excess of 20 g/kg can be seen over large areas of the equatorial belt between 10° N and 10° S. As the tropical disturbance activity of the southern hemisphere increases the large values of surface humidity can be seen to spread over the southwestern Indian Ocean approaching 20° S latitude. Instead of displaying the humidity fields at all other pressure levels we shall next illustrate the monthly mean (humidity based) cloud fields since they describe the climatology more effectively.

3.8 Low, Middle and high Clouds

Cloud fractions are estimated using what are called diagnostic cloud algorithms that are used within the radiative transfer computations, Krishnamurti et al. (1990). Here the differences between the prevailing relative humidity and

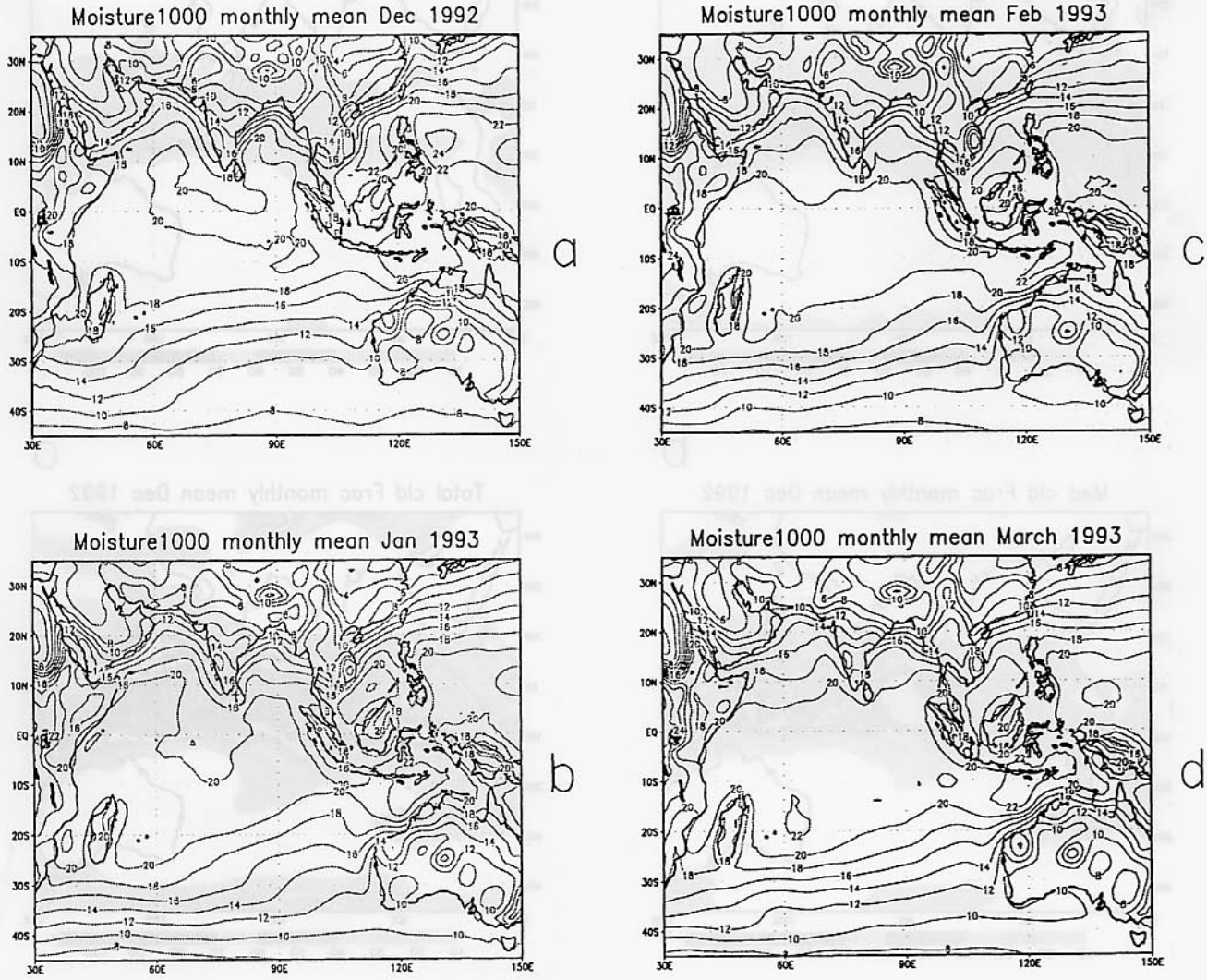

Fig. 10. Monthly mean specific humidity at 1000 mb, for (a) December 1992, 12 UTC (b) January 1993, 12 UTC (c) February 1993, 12 UTC, (d) March 1993, 12 UTC. Units: g/kg; contours interval: 2 g/kg

Table 2. *Threshold Values (Rh_c) of Cloud Types*

Cloud Types	Value
Low	0.66
Medium	0.50
High	0.40

threshold relative humidities are used to define the existence of low, middle and high cloud fractions. Table 2 defines these threshold values. Figures 11–14 illustrate the a) low, b) middle, c) high, and d) total cloud fractions. The ITCZ, in the monthly mean, is characterized by a broad zonal belt of clouds. Cloud fractions generally extend from 10° N to 20° S (and even as far as 30° S during the late winter). Maximum values of the cloud fractions range from 10 to 20% for low clouds, 10 to 90% for middle clouds, 10 to 20%

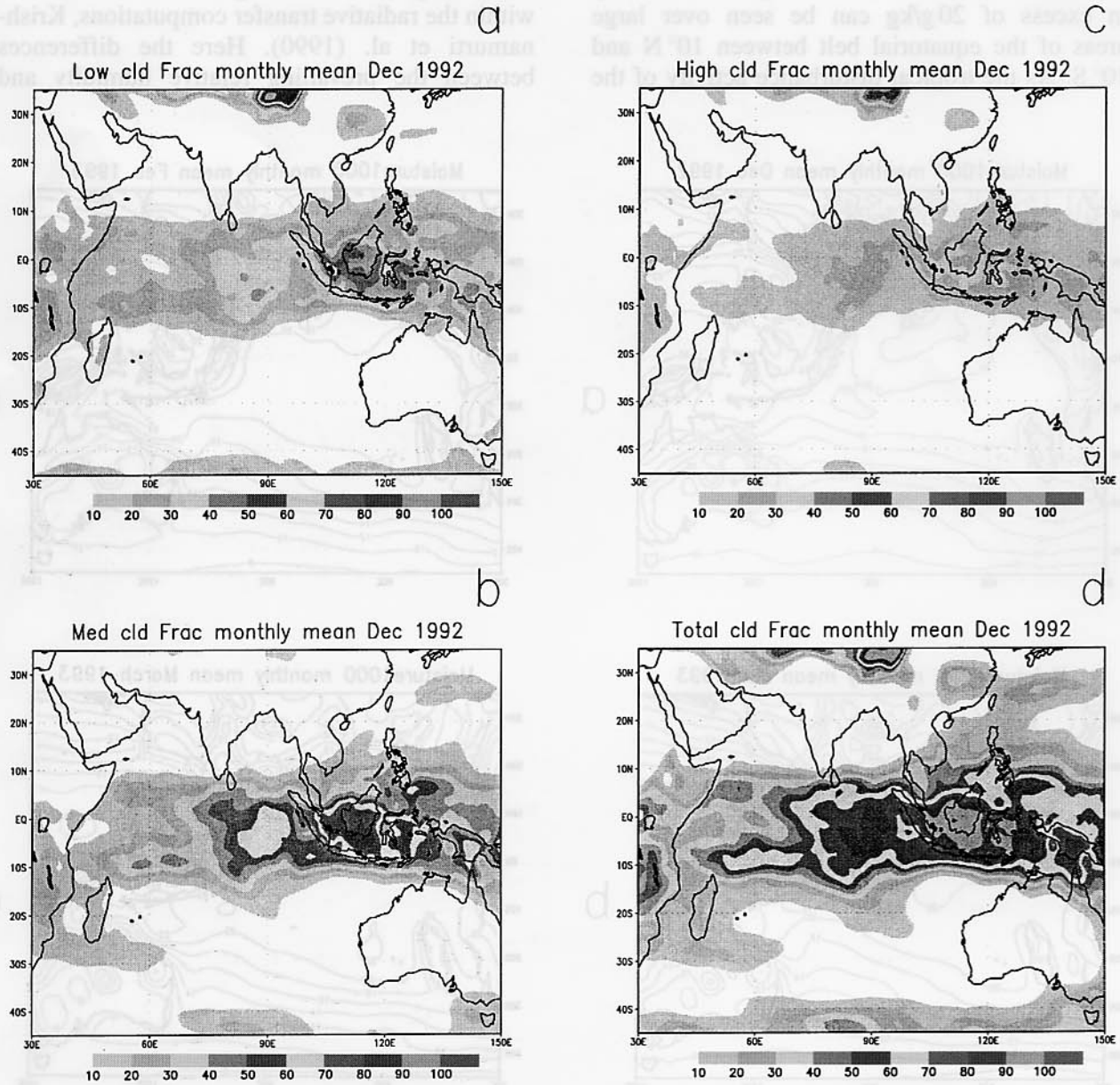

Fig. 11. Monthly mean fractional clouds coverage of sky at 12 UTC for the month of December 1992 (a) low (b) medium (c) high (d) total cloud. Units: %coverage of sky; cloud coverage over shaded area is according to scale shown under each figure

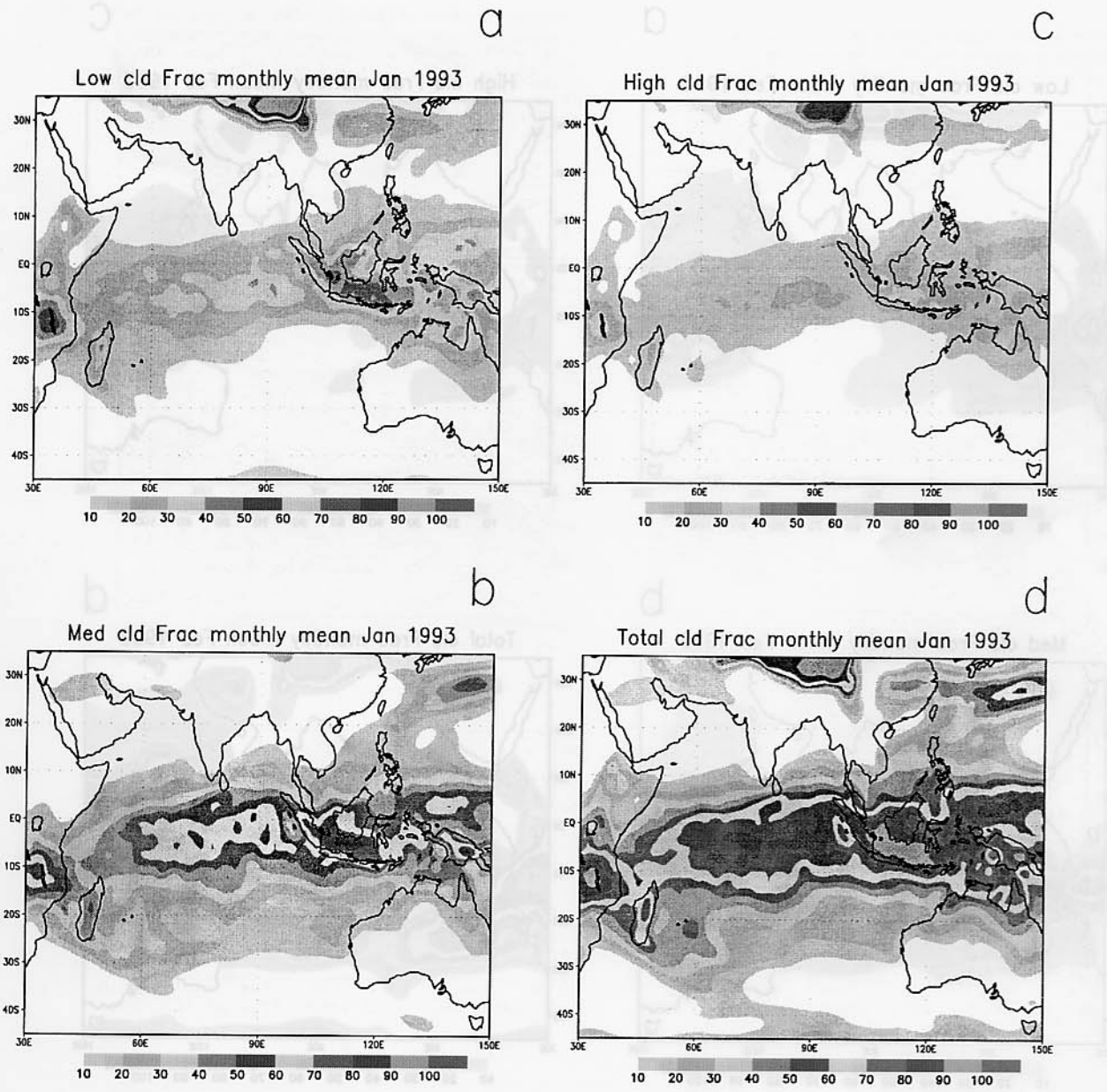

Fig. 12. Monthly mean fractional clouds coverage of sky at 12 UTC for the month of January 1993 (a) low (b) medium (c) high (d) total cloud. Units: %coverage of sky; cloud coverage over shaded area is according to scale shown under each figure

for high clouds and up to 90% for the total cloud cover. Here we make use of a random overlap algorithm for the definition of multiple cloud layers. The surprising result here is the dominance of middle cloud fractions. That result was previously noted by Webster and Stephens (1980) during the winter monsoon experiment of 1978. They stated that a plethora of middle level cloud debris from previous cumulonimbus anvils can descend to middle levels and be long lasting over the moist middle troposphere. This might be a possible explanation for the dominance of the middle clouds. The choice of the threshold relative humidity can easily affect these results, however those were carefully chosen based on line of sight interrogations of middle clouds using satellite based OLR data and atmospheric soundings over the tropics for the FGGE year.

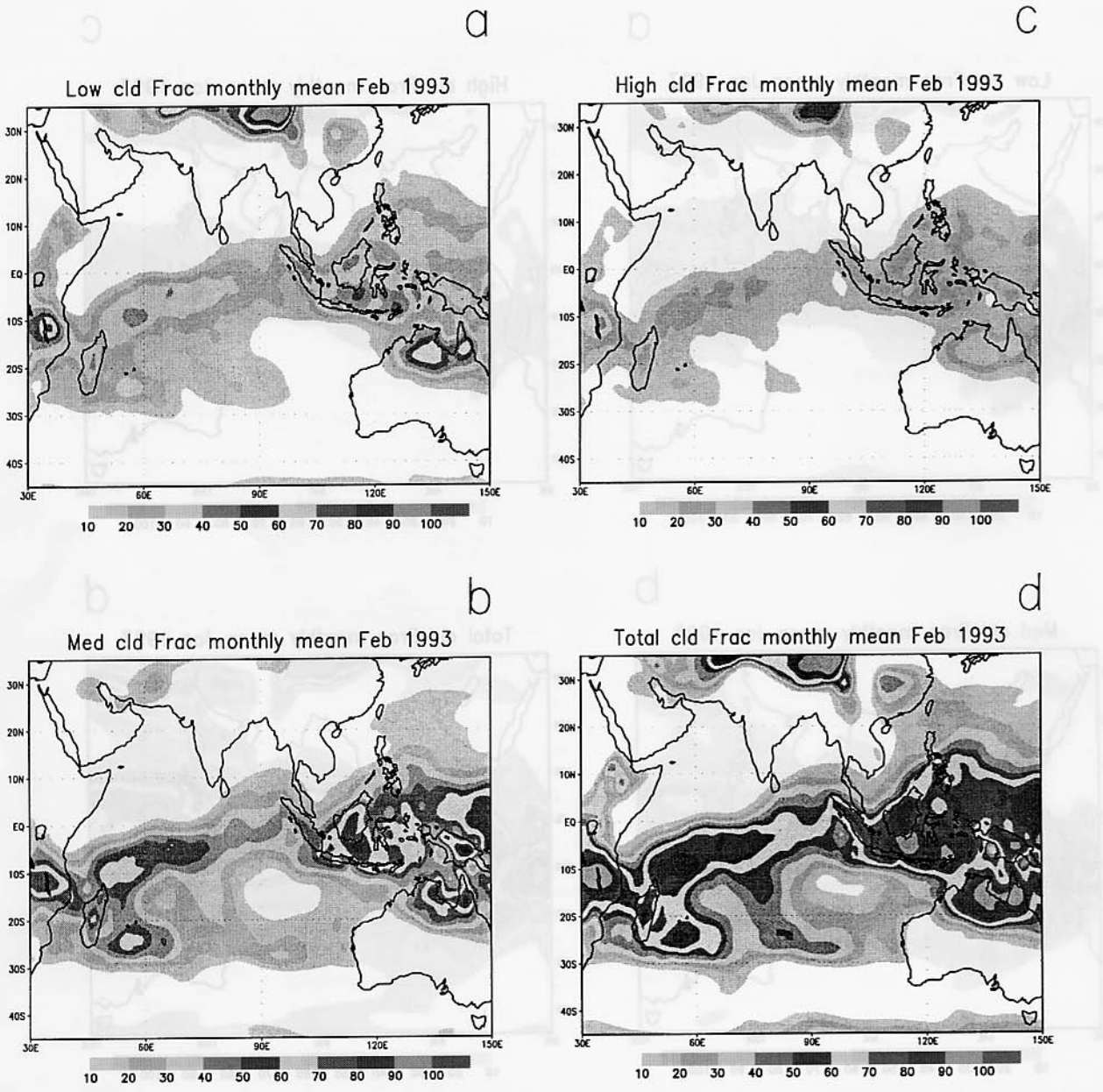

Fig. 13. Monthly mean fractional clouds coverage of sky at 12 UTC for the month of February 1993 (a) low (b) medium (c) high (d) total cloud. Units: %coverage of sky; cloud coverage over shaded area is according to scale shown under each figure

3.9 Surface Fluxes

The monthly mean surface fluxes of latent and sensible heat (for December 1992, January, February and March 1993) are shown in Figs. 15 (a, b, c, d) and 16 (a, b, c, d). Both land and oceanic fluxes are included here, see Krishnamurti et al. (1990) for a discussion of the surface similarity theory. Latent and sensible heat fluxes along the ITCZ are of the order 60 and 10 W/m^2 respectively during December 1992. These monthly mean fluxes increase somewhat during the rest of the winter months to respective values of the order 110 and 15 W/m^2. To the north of the ITCZ the fluxes of latent heat over the northern Arabian sea and the northern Bay of Bengal are the largest. The fluxes over most land masses are small except over northern Australia where values of latent and sensible heat are as large as 130 and 25 W/m^2 respectively during

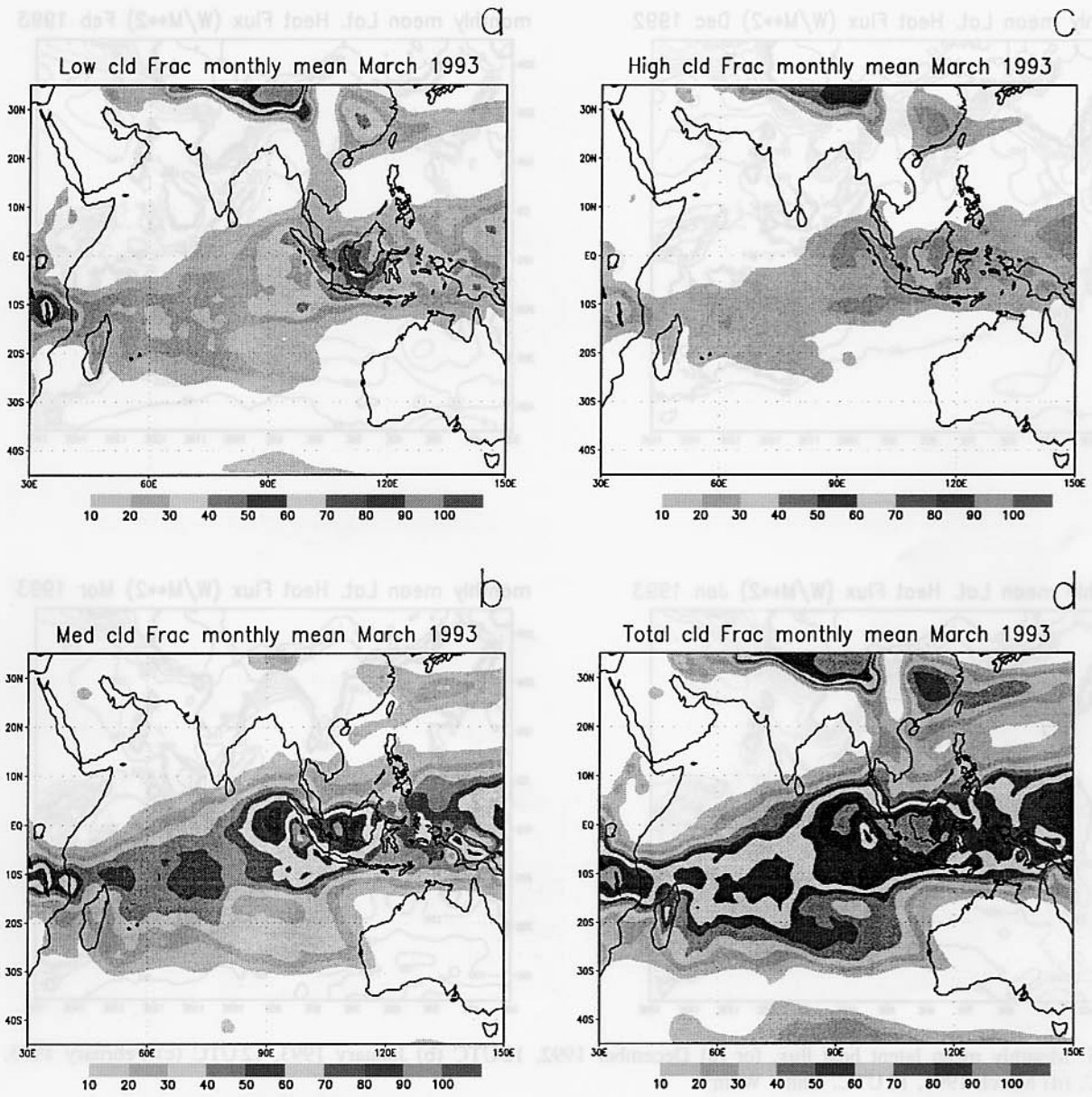

Fig. 14. Monthly mean fractional clouds coverage of sky at 12 UTC for the month of March 1993 (a) low (b) medium (c) high (d) total cloud. Units: %coverage of sky; cloud coverage over shaded area is according to scale shown under each figure

the southern hemisphere summer months. The month to month variability of the fluxes is quite large over the equatorial and southern Indian ocean.

4. Examples of Reanalysis Fields

Here we shall illustrate two separate map times of some sample fields. The reanalysis products (see Table 3) includes both basic model variables and several derived fields as well.

Figure 17 (a, b) illustrates a comparison of the flow fields at 850 mb and superimposed 24 hour rainfall (for 12 UTC on December 1 1992) from the reanalysis and control (that does not include physical initialization). Here the ITCZ is located between 3° N and 5° N. North-easterly flows exhibit a strong eastward turn to the north of the ITCZ. The southeast trades of the southern hemisphere are well defined around 15° S. The physically initialized rainfall is very close to the 'observed' rain, see Fig. 1. The flow field of the

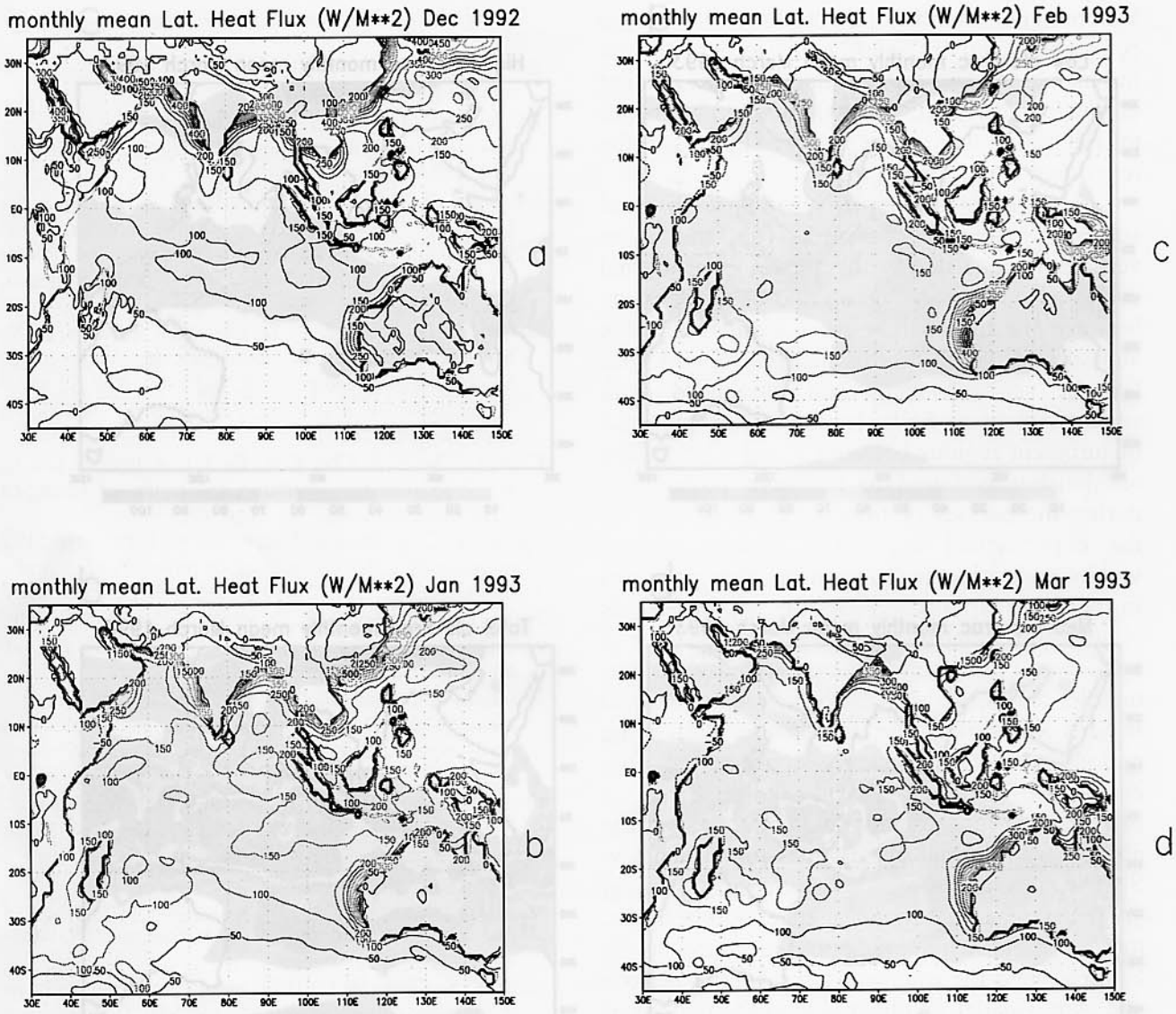

Fig. 15. Monthly mean latent heat flux, for (a) December 1992, 12 UTC (b) January 1993, 12 UTC (c) February 1993, 12 UTC, (d) March 1993, 12 UTC. Units: W/m^2

control is somewhat similar to the physically initialized product however the rainfall described by it is somewhat excessive over most of the equatorial belt. We have noted that the control analysis generally (but not always) underestimates the winter monsoon rainfall. The quality of surface wind analysis is important for the determination of surface fluxes. Typical sample analysis of the surface fluxes of sensible and latent heat for the reanalysis and the control are illustrated in Figs. 18 (a, b) and 19 (a, b). The control analysis overestimates the surface fluxes; the model analysis with physical initialization calls for a weaker evaporation consistent with the lower rainrate input. Excessive evaporation and sensible heat fluxes are conspicuous over many regions especially over the region of the winter monsoon flows over the south China Sea, the ITCZ and the southerly trades along the western Australian Coast. The latent heat fluxes over the

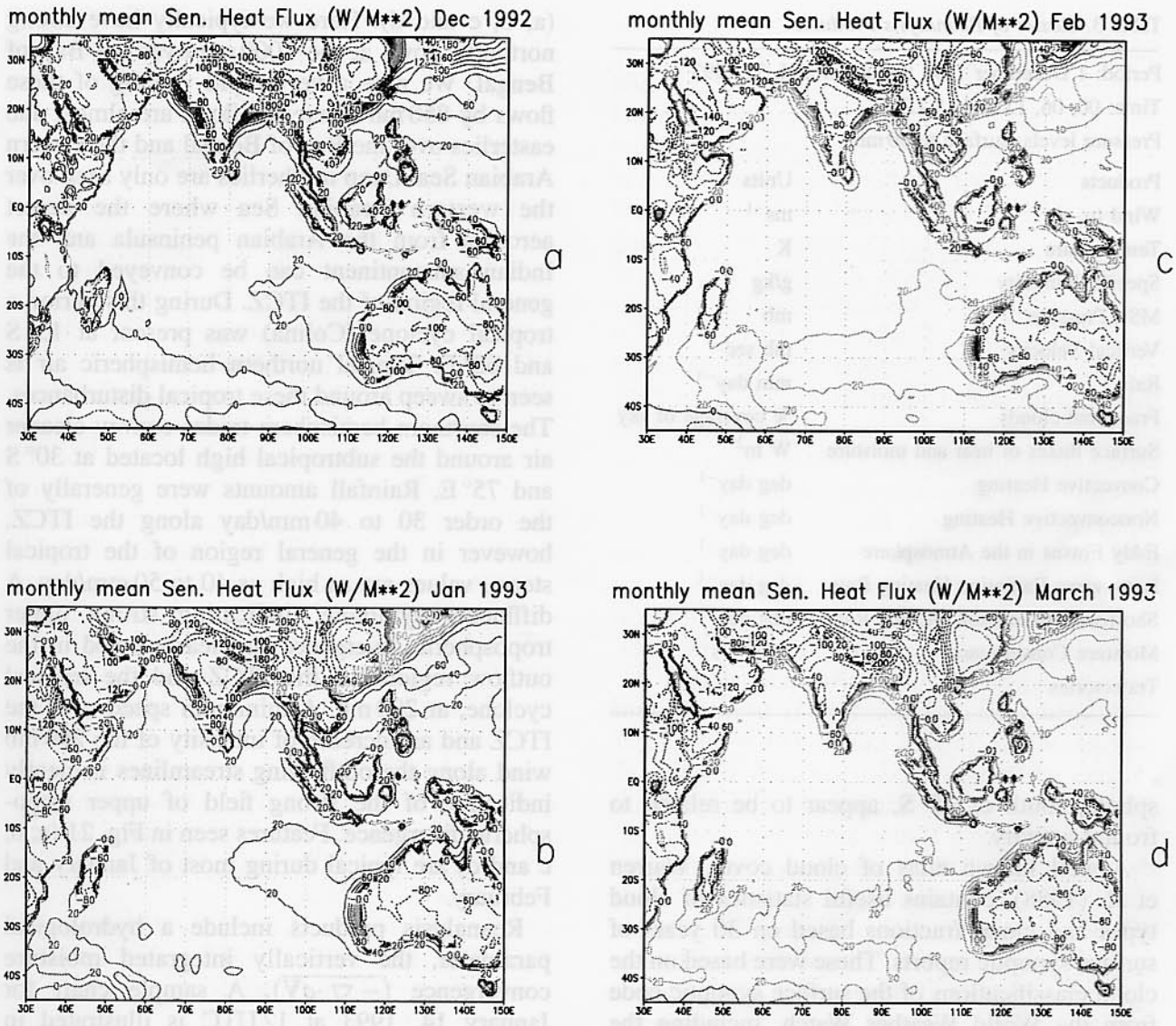

Fig. 16. Monthly mean sensible heat flux, for (a) December 1992, 12 UTC (b) January 1993, 12 UTC (c) February 1993, 12 UTC, (d) March 1993, 12 UTC. Units: W/m^2

ITCZ in the control analysis have values as high as 350 to 400 W/m^2 whereas the reanalysis values are more reasonable ranging between 200 to 250 W/m^2. The sensible heat fluxes from the physically initialized experiment are less than 25 W/m^2, however the control experiment's values appear somewhat excessive, i.e. in the range 25 to 50 W/m^2 over the equatorial latitudes. Typical (model based) cloud fractions deduced from the radiative transfer cloud algorithm (Krishnamurti et al., 1990) are illustrated in Fig. 20 (a, b, c and d). The striking feature is the abundance of middle layer (700 mb to 400 mb) cloud fractions. That, as stated previously, is related to an abundance of long lived middle tropospheric cloud debris from previous cumulonimbus convection that descends and evaporates to the middle troposphere where it is able to sustain itself in a humidity-rich environment. This feature is particularly prominent along the entire length of the ITCZ. The dominant middle level clouds over the southern hemi-

Table 3. *Roster of Reanalysis Products*

Period: 1 December 1992 through March 31 1993	
Time: 00, 06, 12 and 18 UTC	
Pressure levels: surface to 30 mb	
Products	Units
Wind (u, v)	ms^{-1}
Temperature	K
Specific humidity	g/kg
MSL Pressure	mb
Vertical Velocity	mb sec^{-1}
Rain	mm day^{-1}
Fractional clouds	% coverage of sky
Surface fluxes of heat and moisture	W m^2
Convective Heating	deg day^{-1}
Nonconvective Heating	deg day^{-1}
Eddy Fluxes in the Atmosphere	deg day^{-1}
Long-wave Radiation Heating Rate	deg day^{-1}
Short-wave Radiation Heating Rate	deg day^{-1}
Moisture Convergence	g kg^{-1} s^{-1}
Trajectories	

sphere, south of 25° S, appear to be related to frontal activity.

A well known atlas of cloud cover, Warren et al. (1988), contains useful statistics of cloud types and cloud fractions based on 30 years of surface synoptic reports. These were based on the cloud classifications of the surface synoptic code from the World Weather Watch, including the data from the surface ships of opportunity. The COADS data sets were a major source for this project. It is of interest to ask if these data sets for the northern winter months carry a high percentage of middle level cloud cover. This atlas carries statistics on altostratus, nimbostratus and altocumulus. Looking at the region from the equator to 10° S we do find a rich population of middle clouds over the region of the ITCZ during the winter months. The fractions of these cloud types vary geographically between 4% to 65%, with the maximum middle cloudiness occurring between 0600 and 1800 local time. Low cloud fractions lie generally in the range of 20 to 60% over the equatorial belt whereas the high cloud fractions are somewhat less.

A second example of a very active phase of the winter monsoon will be next illustrated in Fig. 21 (a, b, c and d). Here we typically have strong northerly flows at the 1000 mb over the Bay of Bengal. We note a very rapid veering of these flows by 850 mb where the flows are almost due easterlies over the Bay of Bengal and the eastern Arabian Sea. Deep northerlies are only seen over the western Arabian Sea where the desert aerosols from the Arabian peninsula and the Indian subcontinent can be conveyed to the general region of the ITCZ. During this period a tropical cyclone (Colina) was present at 13° S and 62° E. Typical northern hemispheric air is seen to sweep around these tropical disturbances. The sourthern hemisphere trades convey cleaner air around the subtropical high located at 30° S and 75° E. Rainfall amounts were generally of the order 30 to 40 mm/day along the ITCZ, however in the general region of the tropical storm, values are as high as 40 to 50 mm/day. A diffluent asymptote (indicating strong upper tropospheric divergence) is clearly noted in the outflow regions of the ITCZ and the tropical cyclone, at 200 mb. A minimum speed over the ITCZ and an increase of intensity of the 200 mb wind along the outflowing streamlines is clearly indicative of the strong field of upper tropospheric divergence. Features seen in Fig. 21 (a, b, c and d) are typical during most of January and February.

Reanalysis products include a hydrological parameter, the vertically integrated moisture convergence $(\overline{-\nabla \cdot q\mathbf{V}})$. A sample chart for January 14, 1993 at 12 UTC is illustrated in Fig. 22 (a, b). Here the belt roughly between the equator and 10° S shows a net convergence of flux of moisture. The subtropical high of the southern hemisphere is characterized with a divergence of flux of moisture. North of the equator both divergence and convergence of flux of moisture are equally abundant. Specific humidity increases as we proceed towards the ITCZ and as we proceed downwards below 700 mb. We may not see similar fields for the convergence of flux of chemical species since their meridional gradient from the continent to the ocean may be the reverse of that for the moisture, although the vertical gradients may have the same signs as that of the specific humidity.

For this same synoptic period the reanalysed surface fluxes are illustrated in Fig. 23 (a, b).

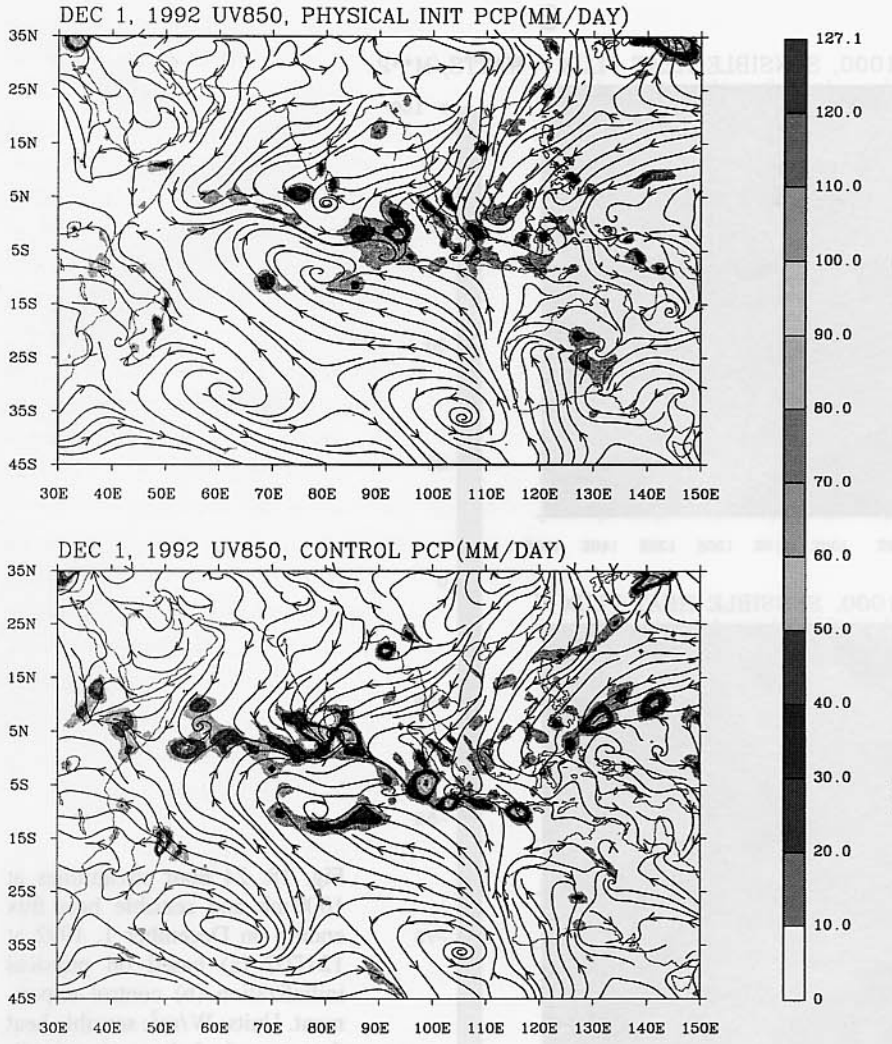

Fig. 17. 24 hours streamlines at 850 mb and rainfall ending on December 1, 1992 at 12 UTC (a) based on physical initialization (b) based on control experiment. Units: mm/day; The rainfall amounts over shaded area are according to the scale shown at the right

Here both the land and oceanic areas are handled by the surface similarity theory that invokes different surface roughness and a coupling of the surface energy balance and the surface similarity theory to determine these fluxes. Sensible heat fluxes are large over Africa and Madagascar. The lateness of the time of day (local time) over most other land masses contributes to lower fluxes of sensible heat. In general the fluxes of sensible heat over the equatorial Indian Ocean are less than 25 W/m^2. The field of latent heat fluxes is the more important field since the Bowen ratio is $\ll 1$. The latent heat flux over the region of the tropical cyclone Colina are large and as high as 400 to 450 W/m^2. In general, values over the southwestern Indian Ocean are quite large. A zonal belt of strong fluxes ($\approx$ 150 to 250 W/m^2) roughly along 10° N extending from the eastern Bay of Bengal to the western Pacific ocean reflects the evaporation arising from the interaction of the northerly colder air streams over warmer oceans and the land mass. The complexity of these features is important for the overall understanding of the winter monsoon over South Asia and these oceans. What we see in Fig. 21 (a, b) are the typical fields during most of the winter monsoon season, i.e. there is a large small scale variability in these fluxes over the western oceans where the effects of air-sea interactions are most prominent.

The components of the instantaneous diabatic heating, within the data assimilation, are func-

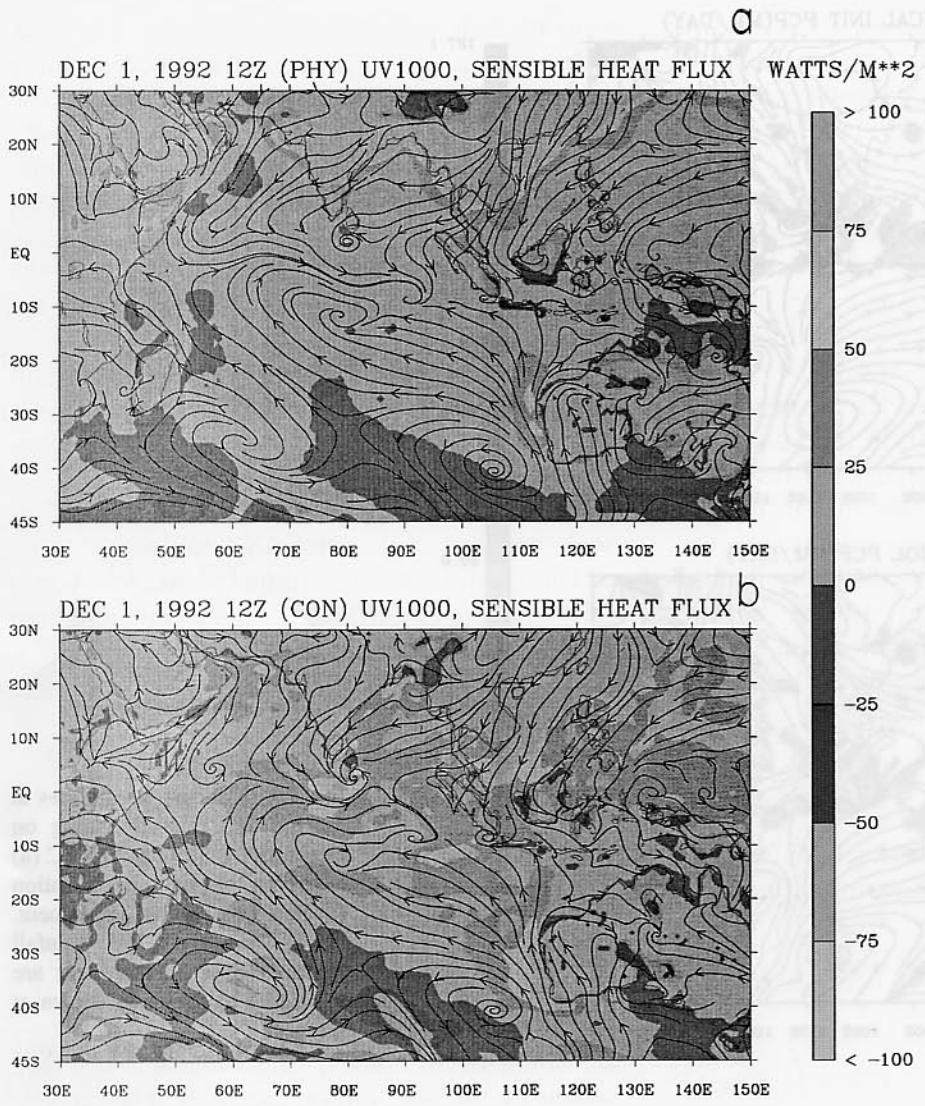

Fig. 18. 24 hour streamlines at 1000 mb and sensible heat flux ending on December 1, 1992 at 12 UTC (a) based on physical initialization (b) control experiment. Units: W/m^2; sensible heat flux over shaded area is according to scale shown

tions of the model parameterization. Here we shall illustrate the vertically integrated instantaneous fields of the following components: (all units are in deg centigrade/day)

a) convective heating, Fig. 24a
b) nonconvective heating, Fig. 24b
c) short-wave radiative heating, Fig. 24c
d) long-wave radiative heating, Fig. 24d
e) total radiative heating, Fig. 24e, and
f) total heating, Fig. 24f

The solar radiation reduces to zero east of India since night time conditions prevail east of 120° E. The field of long-wave radiation shows an essential cooling over most of the winter monsoon region, exceptions include the cloudy region of the ITCZ (see Fig. 24d). Over the ITCZ regions the abundance of middle and total cloud cover appears to lead to both net long-wave flux divergence and a few packets of convergence as well over the troposphere leading to a much weaker cooling and some net warming as well. Thus the cloud radiative effects tend to augment the differential heating of the winter monsoon, i.e. more cooling to the north and south of the ITCZ. The maximum intensities of radiative cooling are of the order 1.5 °C/day; the maximum heating along the ITCZ is of the order 0.4 °C/day. This interesting picture of the radiatively augmented differential heating is further

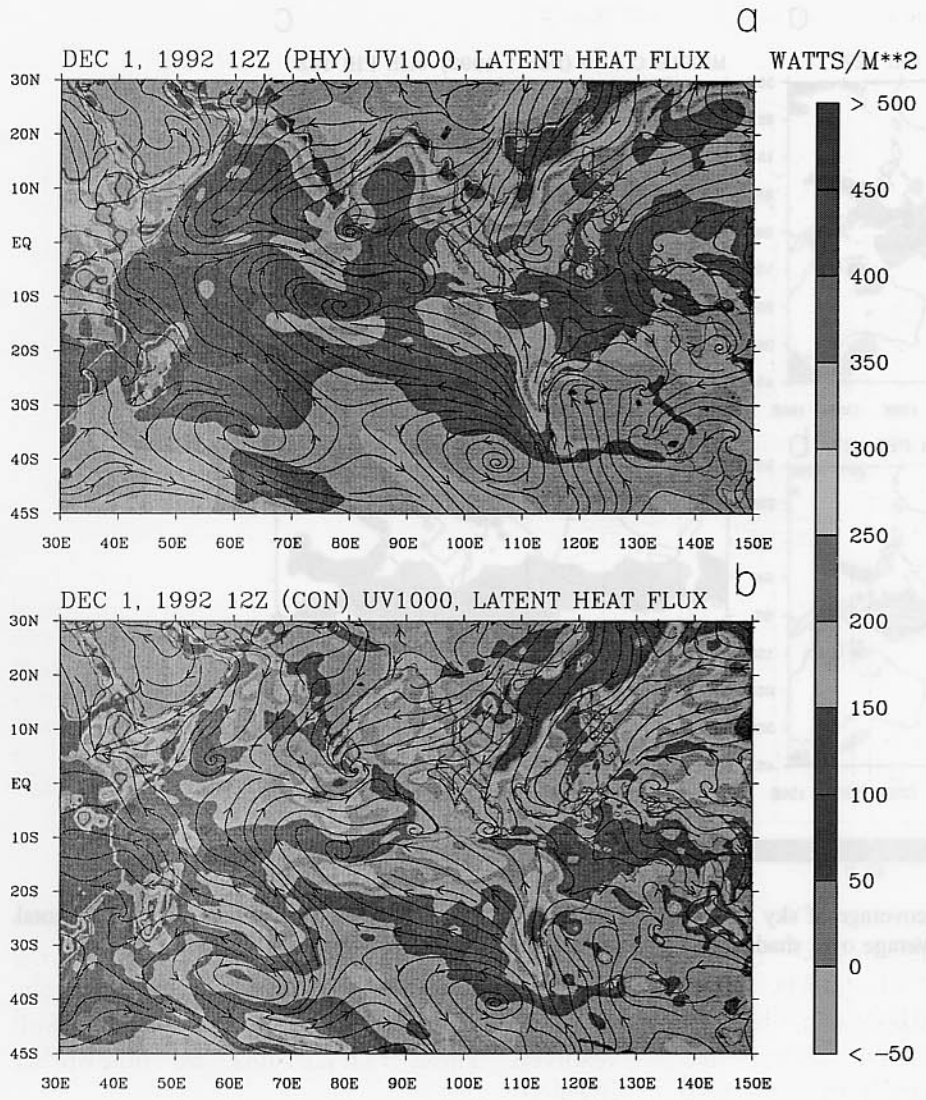

Fig. 19. 24 hour streamlines at 1000 mb and latent heat flux ending on December 1, 1992 at 12 UTC (a) based on physical initialization (b) control experiment

enhanced by the vertically integrated convective heating which is shown in Fig. 24a. The large scale non-convective heating is illustrated in Fig. 24b. We note large values of convective heating which reside over the region of the ITCZ (of the order 5 to 6 °C/day). The distribution of large scale non-convective heating is spotty. This merely identifies regions where the supersaturation is removed over absolutely stable regions where dynamic ascent on the large scale is present. The final picture of the total heating is shown in Fig. 24f. The largest heating amounts prevail over Africa and the equatorial oceanic belt of the ITCZ. This is a net vertically integrated snapshot of heating on December 1, 1992 where the largest values are of the order 4 °C/day over the Indian Ocean. The net heating over most of Africa arises largely from the winter season convection over the equatorial belt and the short wave radiative flux convergence. The largest values are found over the Kenya Highlands and the Kipengere Range of Tanzania where the instantaneous rainfall amounts were very large. Total heating is also large offshore from the Asian coast of China where frontal and convective heating exhibits large values.

Sample vertical distribution of the diabatic heating components as a function of latitude at

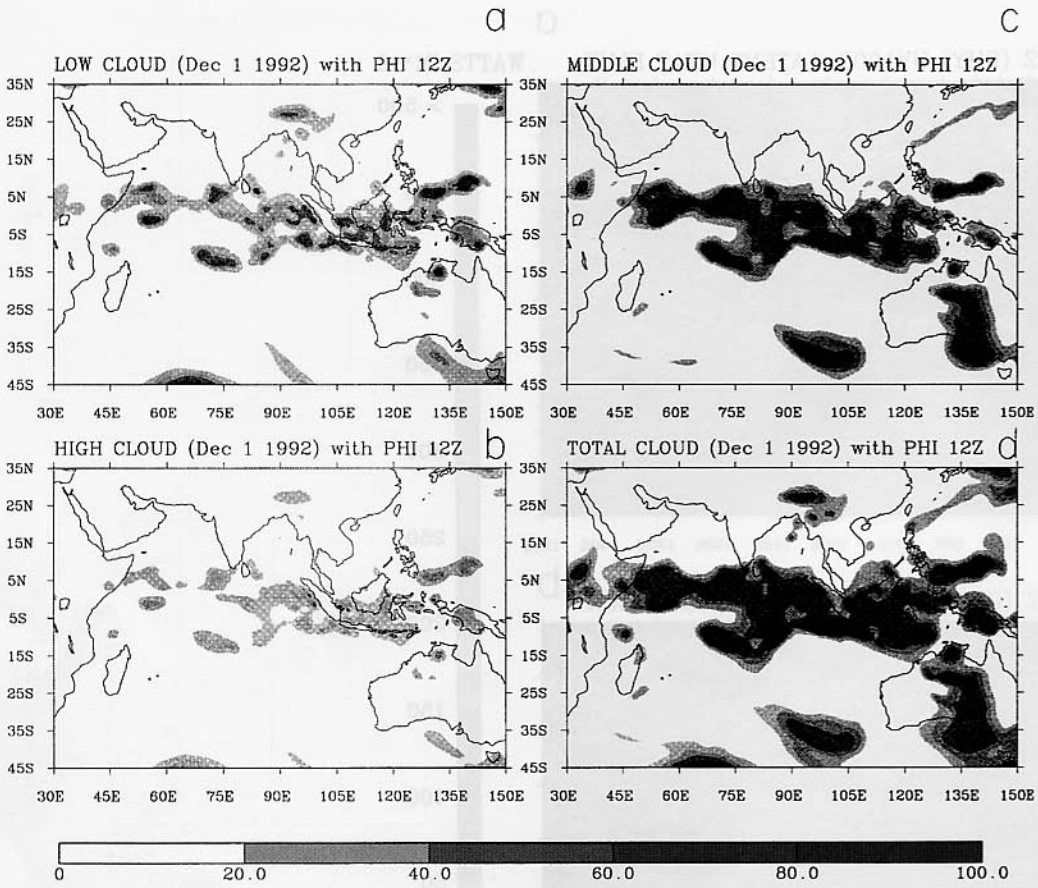

Fig. 20. 24 hour fractional clouds coverage of sky on December 1, 1992, at 12 UTC (a) low (b) medium (c) high (d) total. Units: %coverage of sky; cloud coverage over shaded area is according to scale shown under each figure

75° E are illustrated in Fig. 25 (a, b, c, d, e and f). The units of the analysis here are °C/day. Here we shall look at the ITCZ belt. Over this region convective heating of the order 11 °C/day at around 400 mb is a prominent feature. These are again snapshots from the reanalysis for December 1, 1992 at 12 UTC. The double ITCZ at around ±5° latituds reveals double maxima of heating on either side of the equator. The heating over the southern ITCZ is larger by almost a factor of three compared to its counterpart over the northern hemisphere. The magnitude of the large scale nonconvective heating is weaker over the ITCZ. We also include a vertical distribution of heating contributed by the convergence of eddy heat flux that is largely determined by the model's parameterization of the disposition of surface fluxes (along the vertical) and the vertical diffusion of heat in the thermodynamic equation. This field is weak with the largest heating amounts approaching a degree centigrade per day around 450 mb. The cloud radiative contributions over the ITCZ are some of the most interesting fields. The vertical distribution of short-wave warming along the ITCZ is around 0.2 °C/day below 600 mb and around 1.5 °C/day above the middle clouds at around 400 mb. The longwave radiative flux divergence and accompanying cooling rates of 1 to 2 °C/day are prevalent over most of the troposphere, excep-

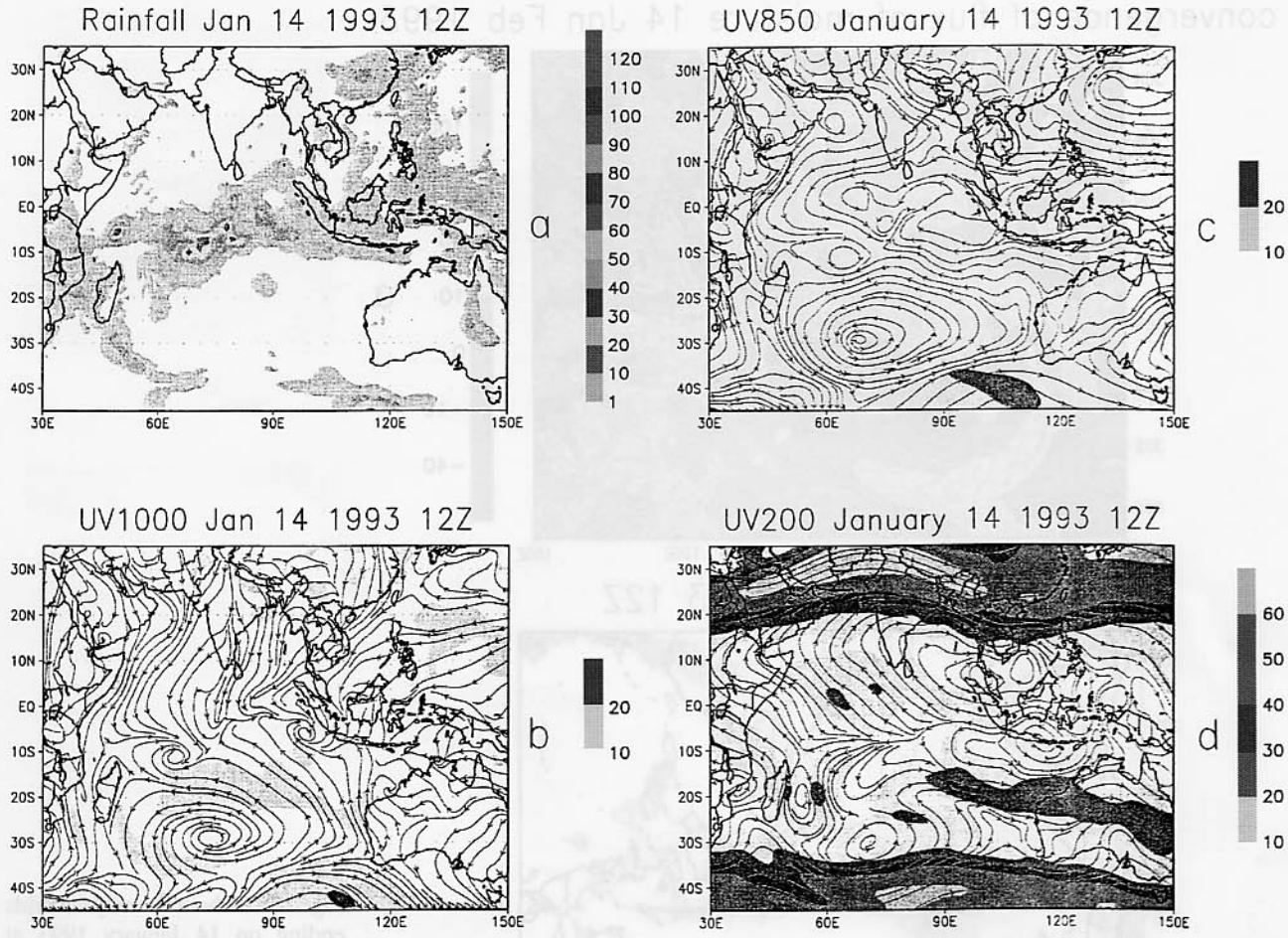

Fig. 21. 24 hour reanalysis fields ending on 14 January 1993 at 12 UTC (a) rainfall (b) streamline and isotach at 1000 mb (c) streamline and isotach at 850 mb (d) streamline and isotach at 200 mb. Units for wind speed: ms^{-1}, units for rainfall: mm/day. Shaded area indicates rainfall amounts and wind speed according to the scale shown below each figure

tions are seen below the middle cloud deck where small longwave warming rates of the order 0.1 to 0.3 °C/day are noted.

Overall the reanalysis provides this quality of 6 hourly fields of diabatic heating that may be useful for the interpretation of the winter monsoon.

5. Concluding Remarks

A global reanalysis at a resolution T170 (that has a transform grid separation of roughly 70 km) provides a strong relationship between the precipitation and the large scale dynamics. That is facilitated by the use of physical initialization which incorporates the observed rainfall (based on satellite products) in the data assimilation presented here. A motivation for this study was to provide the meterological experiment, called INDOEX, over the Indian Ocean. The reanalysis includes 6 hourly fields of wind, temperature, pressure, humidity, rainfall, clouds and a host of derived fields related to the heat sources and sinks of the winter monsoon.

This paper discusses the monthly mean fields for December 1992, January, February and March 1993. These fields show that the winter monsoon flows emanating from the land mass of Asia are in fact very shallow northerlies that turn rapidly and have a strong westerly component as

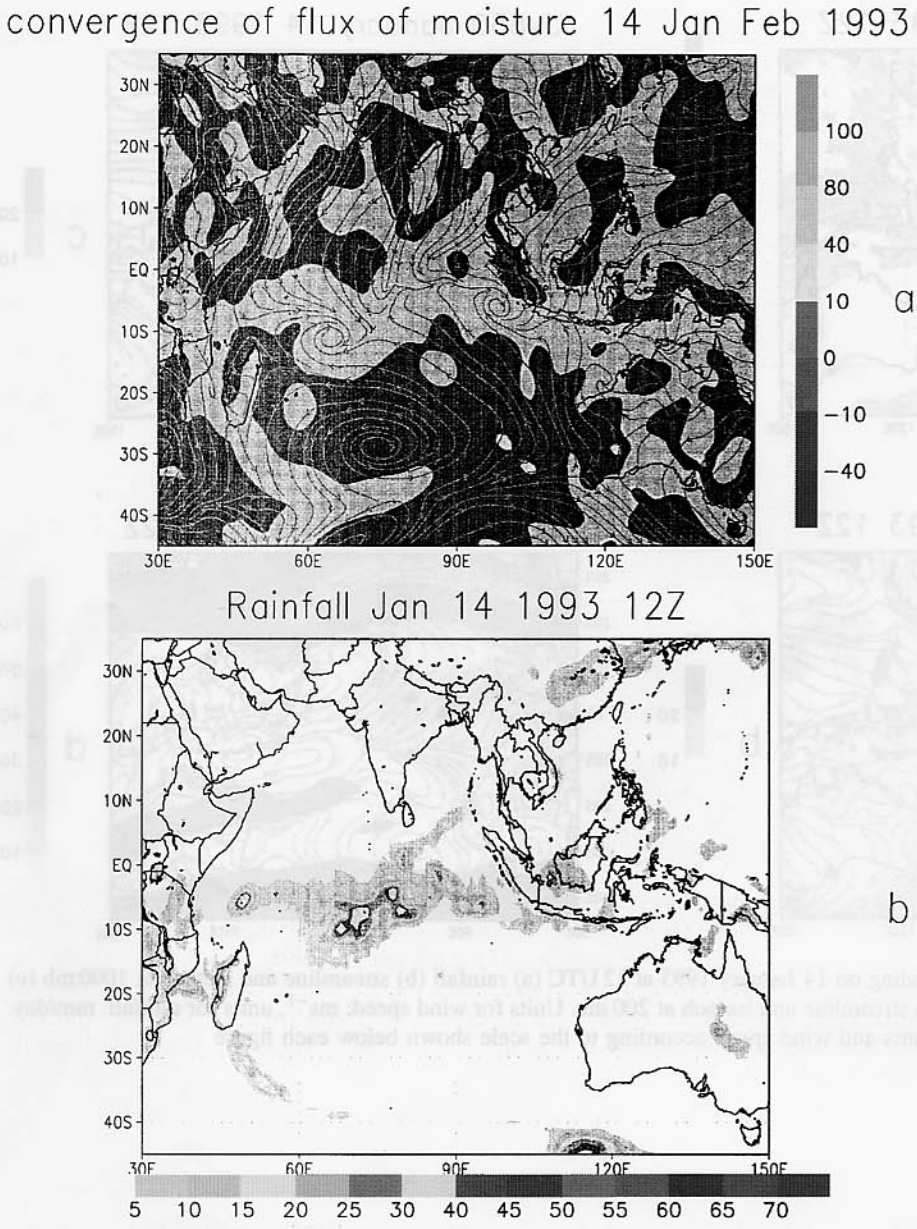

Fig. 22. 24 hour reanalysis fields ending on 14 January 1993 at 12 UTC (a) vertical integrated moisture convergence and 1000 mb streamline (b) rainfall. Units of moisture convergence: $g\,kg^{-1}\,s^{-1}$. Units of rainfall: mm/day; shaded area indicates moisture convergence and rainfall amounts according to the scale shown

we proceed from the sea level to about 2 km. The depth of the monsoonal flow increases in the vicinity of the ITCZ near the equator. The diurnal change in the depth of the inversion layer is fairly pronounced over the land mass of south Asia; that plus the rapid veering of wind with height has important implications on the diurnal change of pollution transports from the north towards the ITCZ.

This paper also includes a display of some daily fields that show the importance of transient motion over this region. The salient features in the daily maps include the converging monsoonal and trade wind systems of the two hemispheres and a plethora of tropical disturbances to the south of the ITCZ. In the upper troposphere this region shows a pronounced diffluent flow with two pronounced anticyclonic systems in each hemisphere. Among the other daily fields the diagnostically deduced cloud fields were most interesting. Our assimilation points to a maximum in the middle tropospheric middle cloud

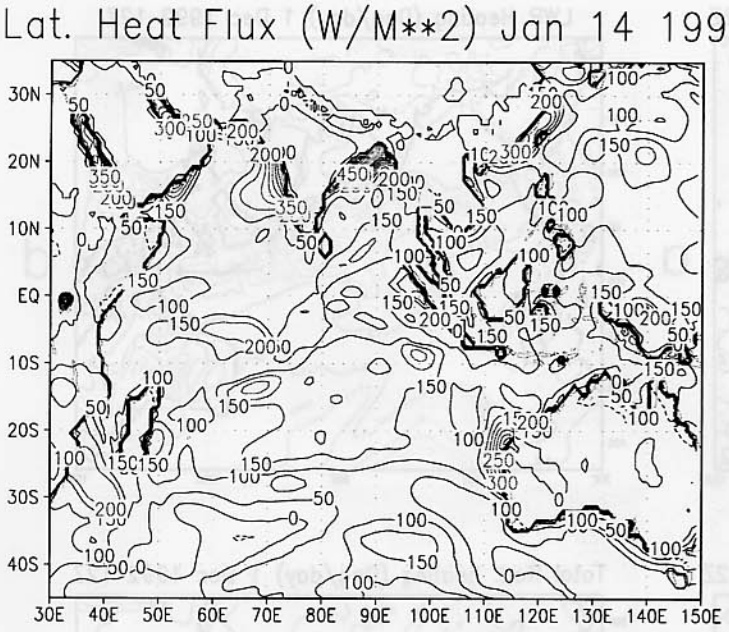

a

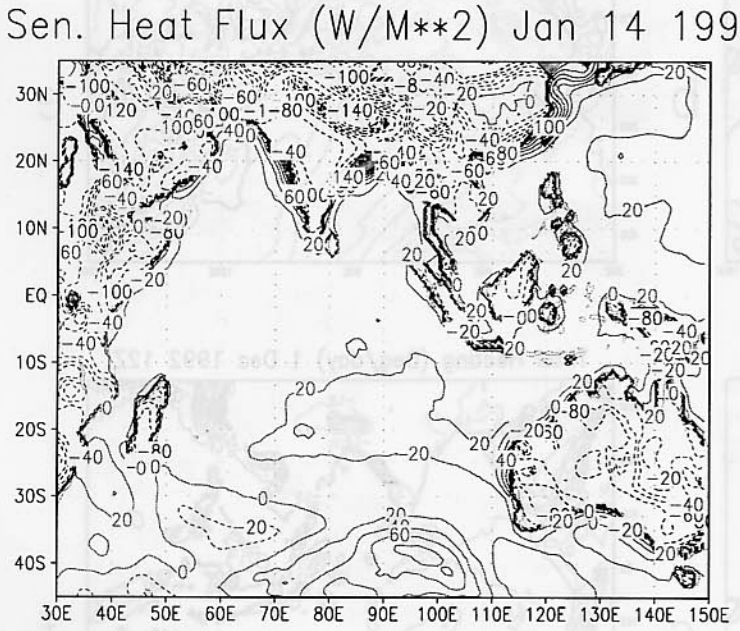

b

Fig. 23. 24 hours reanalysis surface fluxes ending on 14 January 1993 at 12 UTC (a) latent heat flux (b) sensible heat flux. Units: W/m^2

fractions. Such a result has been suggested in previous studies of Webster and Stephens (1980) over the winter monsoon domain. We feel that this region is fairly moist and can maintain middle clouds for long periods of time against entertainment of any dry air from surrounding regions. Deep cumulus convection, once initiated, appears to abate and appear as a middle tropospheric long-lasting (and more precipitating) cloud debris. This is an area that may require observational confirmation during INDOEX. Our analysis also includes a display of some of the

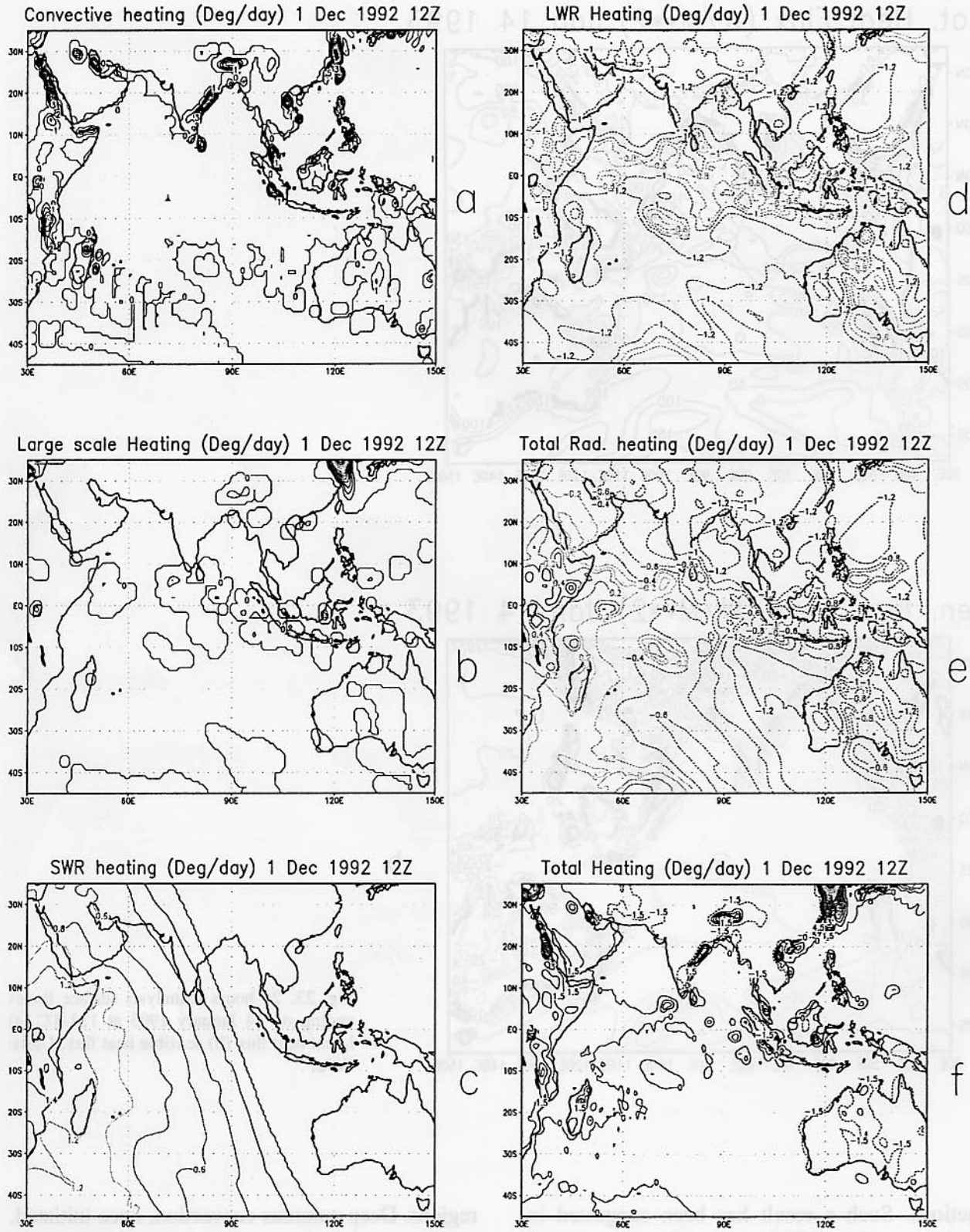

Fig. 24. 24 hours reanalysis diabatic heating ending on 1 December, 1992 at 12 UTC: (a) convective heating; contour intervals: 1.0 deg/day; (b) large-scale heating; contour intervals: 0.2 deg/day; (c) SW radiation heating; contour intervals: 0.2 deg/day; (d) LW radiation heating; contour intervals: 0.2 deg/day; (e) total radiative heating; contour intervals: 0.2 deg/day; (f) total heating; contour intervals: 1.5 deg/day; units: deg/day

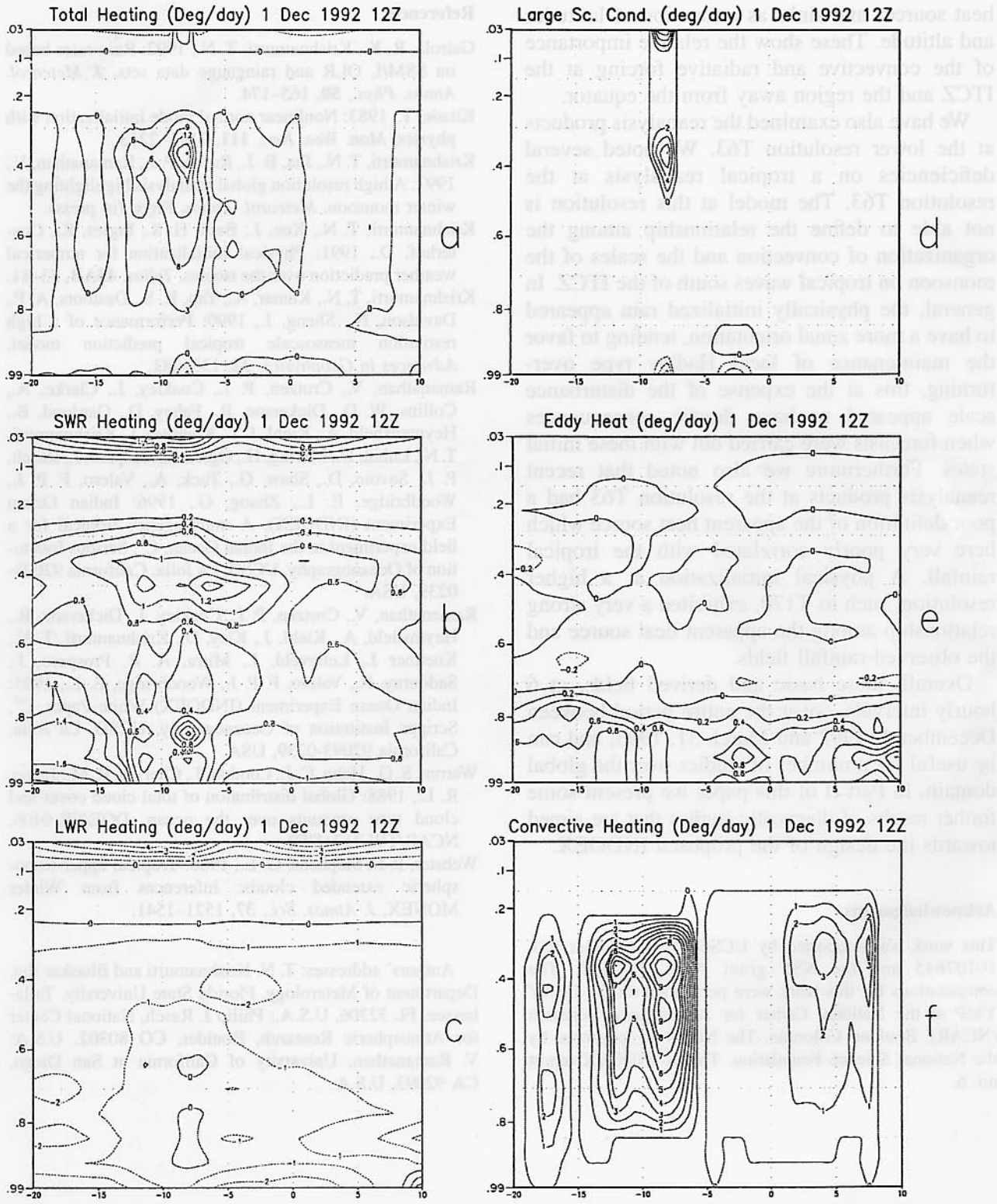

Fig. 25. Cross-section of reanalysis diabatic heating at 75° E ending on 1 December 1992 at 12 UTC: (a) total heating; contour intervals: 3 deg/day; (b) SW radiation heating; contour intervals: 0.2 deg/day; (c) LW radiation heating; contour intervals: 1 deg/day; (d) large-scale condensation; contour intervals: 2 deg/day; (e) eddy heat; contour intervals: 0.2 deg/day; (f) convective heating; contour intervals: 1 deg/day; units: deg/day

heat sources and sinks as a function of latitudes and altitude. These show the relative importance of the convective and radiative forcing at the ITCZ and the region away from the equator.

We have also examined the reanalysis products at the lower resolution T63. We noted several deficiencies on a tropical reanalysis at the resolution T63. The model at this resolution is not able to define the relationship among the organization of convection and the scales of the monsoon on tropical waves south of the ITCZ. In general, the physically initialized rain appeared to have a more zonal orientation, tending to favor the maintenance of local Hadley type overturning, this at the expense of the disturbance scale appeared to have drastic consequences when forecasts were carried out with these initial states. Furthermore we also noted that recent reanalysis products at the resolution T63 had a poor definition of the apparent heat source which here very poorly correlated with the tropical rainfall. A physical initialization at a higher resolution, such as T170, exhibited a very strong relationship among the apparent heat source and the observed rainfall fields.

Overall, these basic and derived fields, at 6 hourly intervals, cover the entire period between December 1, 1992 and March 31, 1993, and can be useful for a number of studies over the global domain. In Part II of this paper we present some further results of diagnostic studies that are aimed towards the design of the proposed INDOEX.

Acknowledgments

This work was supported by UCSD-C^4 NSF Grant P.O. 10107645 and the NSF grant ATM 9312537. The computations for this work were performed on the CRAY YMP at the National Center for Atmospheric Research (NCAR), Boulder, Colorado. The NCAR is sponsored by the National Science Foundation. This is INDOEX report no. 6.

References

Gairola, R. K., Krishnamurti, T. N., 1992: Rain rates based on SSM/I, OLR and raingauge data sets. *J. Meteorol. Atmos. Phys.*, **50**, 165–174.

Kitade, T., 1983: Nonlinear normal mode initialization with physics. *Mon. Wea. Rev.*, **111**, 2194–2213.

Krishnamurti, T. N., Jha, B. J., Rasch, P. J., Ramanathan, V., 1997: A high resolution global reanalysis highlighting the winter monsoon. *Meteorol. Atmos. Phys.* (in press).

Krishnamurti, T. N., Xue, J., Bedi, H. S., Ingles, K., Oosterhof, D., 1991: Physical initialization for numerical weather prediction over the tropics. *Tellus*, **43AB**, 53–81.

Krishnamurti, T. N., Kumar, A., Yap, K. S., Dastoors, A. P., Davidson, N., Sheng, J., 1990: Performance of a high resolution measoscale tropical prediction model. *Advances in Geophysics*, **32**, 133–281.

Ramanathan, V., Crutzen, P. J., Coakley, J., Clarke, A., Collins, W. D., Dickerson, R., Fahey, D., Gardoud, B., Heymensfield, A., Kiehl, J. T., Kuettner, J., Krishnamurti, T. N., Lubin, D., Maring, H., Ogren J., Prospero, J., Rasch, P. J., Savoie, D., Shaw, G., Tuck, A., Valero, F. P. J., Woodbridge, E. L., Zhang, G., 1996: Indian Ocean Experiment (INDOEX), A multi-agency tropical for a field experiment in the Indian Ocean, C^4, Scripps Institution of Oceanography, UCSB, La Jolla, California 92093-0239, USA.

Ramanathan, V., Crutzen, P. J., Coakley, J., Dickerson, R., Heymsfield, A., Kiehl, J., Kley, D., Krishnamurti, T. N., Kuettner J., Lelieveld, J., Mitra, A. P., Prospero, J., Sadourny, R., Valero, F. P. J., Woodbridge, E. L., 1995: Indian Ocean Experiment (INDOEX) White Paper, C^4, Scripps Institution of Oceanography, UCSD, La Jolla, California 92093-0239, USA.

Warren, S. G., Hahn, C. J., London, J., Chervin, R. M., Jenne, R. L., 1988: Global distribution of total cloud cover and cloud type amounts over the ocean. DOE/ER-0406, NCAR/TW-317+STR.

Webster, P. J., Stephens, G. L., 1980: Tropical upper-tropospheric extended clouds: inferences from Winter MONEX. *J. Atmos. Sci.*, **37**, 1521–1541.

Authors' addresses: T. N. Krishnamurti and Bhaskar Jha, Department of Meterology, Florida State University, Tallahassee, FL 32306, U.S.A.; Philip J. Rasch, National Center for Atmospheric Research, Boulder, CO 80302, U.S.A; V. Ramanathan, University of California at San Diego, CA 92093, U.S.A